

# APPROXIMATION OF SURFACE DIFFUSION FLOW: A SECOND ORDER VARIATIONAL CAHN–HILLIARD MODEL WITH DEGENERATE MOBILITIES

ELIE BRETIN, SIMON MASNOU, ARNAUD SENEGERS, AND GARRY TERII

ABSTRACT. This paper tackles the approximation of surface diffusion flow using a Cahn–Hilliard-type model. We introduce and analyze a new second order variational phase field model which associates the classical Cahn–Hilliard energy with two degenerate mobilities. This association allows to gain an order of approximation of the sharp limit. In a second part, we propose some simple and efficient numerical schemes to approximate the solutions, and we provide numerical 2D and 3D experiments that illustrate the interest of our model in comparison with other Cahn–Hilliard models.

## 1. INTRODUCTION

This paper addresses the approximation of surface diffusion flow, which is the evolution of a time-dependent surface  $\Gamma : t \mapsto \Gamma(t)$  moving with normal velocity at every time  $t$ :

$$V(t) = \Delta_{\Gamma(t)} H(t),$$

where  $H(t)$  is the mean curvature vector on  $\Gamma(t)$ , and  $\Delta_{\Gamma(t)}$  the Laplace–Beltrami operator defined on the surface. For simplicity, we shall frequently omit the time dependence.

The starting point of our approximation model is the classical Cahn–Hilliard equation

$$\varepsilon^2 \partial_t u = \Delta (W'(u) - \varepsilon^2 \Delta u),$$

where  $u : (t, x) \mapsto u(t, x)$  is a smooth function whose level surface  $\{u(t, \cdot) = \frac{1}{2}\}$  approximates  $\Gamma(t)$ ,  $\varepsilon > 0$  is a small parameter, and  $W$  is a reaction potential, typically  $W(s) = \frac{1}{2} s^2 (1 - s)^2$ .

The Cahn–Hilliard equation has been introduced as a mathematical model for phase separation and phase coarsening in binary alloys [15, 17], but it has also been used for applications as diverse as the modeling of two evolving components of intergalactic material or the description of a bacterial film, see the references in [34], or the modeling of multiphase fluid flows [7, 8]. More recently it was proposed as an inpainting model in image processing, see [6, 14, 21]. We refer to [34] for an inspiring general introduction to the Cahn–Hilliard equation, see also the recent book [32] where state-of-art results and many applications of the Cahn–Hilliard equation are presented.

### Sharp interface limit and mobilities.

Pego determined with formal arguments in [35], and Alikakos et al proved rigorously in [3], that the sharp limit flow of the Cahn–Hilliard equation (for suitable time regimes as  $\varepsilon \rightarrow 0$ ) is the Mullins–Sekerka interface motion.

Observe now that the Cahn–Hilliard equation can be equivalently written as

$$(1) \quad \varepsilon^2 \partial_t u = \operatorname{div} (M(u) \nabla (W'(u) - \varepsilon^2 \Delta u))$$

with the particular choice  $M(u) \equiv 1$ . If  $M$  is now chosen to be non constant, it plays the role of a concentration-dependent mobility. Cahn et al. showed formally in [16] that if one uses a

---

2020 *Mathematics Subject Classification.* 74N20, 35A35, 53E10, 53E40, 65M32, 35A15.

*Key words and phrases.* Phase field approximation, Cahn–Hilliard equation, surface diffusion, degenerate mobilities, numerical approximation.

degenerate mobility  $M(u) = u(1 - u)$  (degenerate in the sense that there is no motion where  $u = 0$  or  $1$ ) and a logarithmic potential

$$W(s) = \frac{1}{2}\theta [s \ln(s) + (1 - s) \ln(1 - s)] + \frac{1}{2}s(1 - s),$$

the sharp limit motion is the surface diffusion flow. However, the singularity of such a logarithmic potential makes the model not well suited for numerical simulations. We shall see in this paper that a different model can be proposed which leads to the surface diffusion flow as well, but involves rather the smooth potential

$$W(s) = \frac{s^2(1 - s)^2}{2}.$$

The choice of appropriate degenerate mobility and potential is important. It was observed in the review paper [29] that some choices lead to inconsistencies, in the sense that depending on how terms are identified in the matched asymptotic analysis expansion, one can either show the convergence to surface diffusion flow, or to a stationary flow with null velocity. The authors of [30, 31] suggested that such inconsistencies come from the presence of an additional bulk diffusion term in the limit motion, i.e. the limit velocity is:

$$V = \frac{2}{3}\Delta_\Gamma H + \alpha H \nabla_n H$$

This has been corroborated numerically in [22, 23] where undesired coarsening effects are observed. The additional term in the velocity depends on the derivative of the mobility  $M'(u_0)$ , where  $u_0$  is the outer solution in the matched asymptotics which equal 0 or 1. To obtain a pure motion by surface diffusion, one needs to take a higher order mobility, for example  $M(s) = s^2(1 - s)^2$  [31]. With such a choice, the bulk diffusion appears in higher order terms and the correct velocity is recovered (with a different multiplicative constant):

$$V = \alpha \Delta_\Gamma H$$

These conclusions have been extended to the anisotropic case in [25].

### Positivity property and order of phase field model.

We now turn to the following question: starting from an initial  $u(0)$  with values in  $[0, 1]$  and using the above mobility, does the solution  $u$  remain valued in  $[0, 1]$ ? This is often referred to as the *positivity condition* as it implies that all phase functions remain positive in a multiphase context. This condition is important also because it means the function remains within the pure state phase boundaries.

The theoretical results of [31, 40] and the numerical evidences of [22, 23] establish that it is not the case with the Cahn–Hilliard model with mobility (1). More precisely the profile of the solution shows some oscillations when reaching the pure states. This comes from the influence in the asymptotic expansion of the solution of the first order error term which does not vanish for this kind of phase field models.

To circumvent this problem a non variational model has been introduced in [36]:

$$(2) \quad \begin{cases} \varepsilon^2 \partial_t u = \operatorname{div} (M(u) \nabla \mu) \\ g(u) \mu = W'(u) - \varepsilon^2 \Delta u \end{cases}$$

with  $g(s) = \gamma |s|^p |1 - s|^p$ ,  $p \geq 0$ .

The idea is to add another degenerate term  $g$  that acts as a diffusion preventing term and forces the aforementioned error term to be smaller and to converge to zero far from the interface. This model is known to achieve better numerical accuracy than the classical model (1), and it has been successfully adapted in various applications, see for example [1, 33, 38, 37].

Several choices have been made for  $p$ , the most acclaimed ones being  $p = 1$  and  $p = 2$  but they were motivated by better numerical results rather than from a theoretical standpoint. In this paper we explain why  $p = 1$  is the correct choice as it imposes the leading error term of the solution to be zero. This result is new to the extent of our knowledge.

While it has excellent numerical properties, the above model (2) does not derive from an energy and it is thus more difficult to prove rigorously theoretical properties and to extend the model to complex multiphase applications. Therefore, a variational adaptation is proposed in [40]:

$$\begin{cases} \varepsilon^2 \partial_t u = \operatorname{div} (M(u) \nabla \mu) \\ \mu = g(u) W'(u) - \varepsilon^2 \operatorname{div} (g(u) \nabla u) + g'(u) \left( W'(u) + \frac{\varepsilon^2}{2} |\nabla u|^2 \right) \end{cases}$$

The idea is to inject the second degeneracy  $g$  in the energy. The model conserves the same advantages as the non variational version, in particular the fact that the choice  $p = 1$  remains the correct one and nullifies the leading error term of the solution. However it relies on changing the energy, thus making it harder to extend to complex multiphase application or to add an anisotropy. Also, it seems more appropriate to incorporate the mobility in the metric rather than in the geometry of the evolution problem. This is what we propose in this paper.

### A new variational Cahn–Hilliard model of order two.

Like in [40], we want to approximate the surface diffusion flow using a second order variational phase field model, but we want it closer to the original Cahn–Hilliard model.

The new Cahn–Hilliard model we propose reads as:

$$\begin{cases} \varepsilon^2 \partial_t u &= N(u) \operatorname{div} (M(u) \nabla (N(u) \mu)) \\ \mu &= W'(u) - \varepsilon^2 \Delta u, \end{cases}$$

and at least in the case where

$$W(s) = \frac{1}{2} s^2 (1-s)^2, \quad M(s) = s^2 (1-s)^2 \text{ and } N(s) = \frac{1}{s(1-s)},$$

we will show that this model is of order two and converges to the surface diffusion flow. Consequently, this model has all desired properties while conserving the correct energy to dissipate.

Moreover, as the conservation of volume is one key feature of the Cahn–Hilliard equation, we review how well each model manages to preserve this property. Furthermore, because of the higher consistency of the solution profile, we will show that we achieve very good numerical approximation in this area as in [9, 13].

**Outline of the paper:** The paper is organized as follows. First, we review in Section 2 the properties of the Cahn–Hilliard model with mobility and the drawbacks that need to be improved. In Section 3 we present our new variational Cahn–Hilliard model and review its properties. We prove these properties in Section 4 using the formal method of matched asymptotic expansion. The necessary tools are presented at the beginning of the proof. In the numerical section 5, we first explain how to derive a simple and efficient scheme using a convex splitting of Cahn–Hilliard energy and exploiting the variational mobility structure. Finally, we propose some numerical experiments that compare the various Cahn–Hilliard models and highlight the advantages of our new model.

## 2. REVIEW OF THE PROPERTIES OF THE CAHN–HILLIARD EQUATION WITH MOBILITY

In this section we summarize the properties of the existing models and explain why we will introduce a new one in the next section. A motion by surface diffusion can be obtained as the sharp limit of the Cahn–Hilliard equation with mobility if we choose a mobility  $M$  that is of sufficiently high order.

### 2.1. The Cahn–Hilliard model with mobility to approximate surface diffusion flow.

We recall that the normal velocity associated with a surface diffusion flow is:

$$V = \Delta_\Gamma H$$

We also recall that, if  $\Omega$  denotes the inner domain enclosed by  $\Gamma$ , the phase field method consists in approximating the characteristic function  $\mathbb{1}_\Omega$  by a smooth function of the form  $u_\varepsilon = q(\text{dist}(\cdot, \Omega)/\varepsilon)$  where  $q$  is the so-called *optimal profile* associated with the potential  $W$ ,  $\varepsilon$  represents the thickness of the smooth transition from 0 to 1, and  $\text{dist}$  denotes the signed distance function. The one associated with our choice  $W(s) = \frac{1}{2}s^2(1-s)^2$  verifies the following properties:

$$(3) \quad \begin{cases} q(z) = \frac{1 - \tanh(z)}{2} \\ q'(z) = -\sqrt{2W(q)} \\ q''(z) = W'(q) \end{cases}$$

We denote:

$$\begin{cases} c_W = \int_{\mathbb{R}} (q'(z))^2 dz = \frac{1}{6} \\ c_M = \int_{\mathbb{R}} \frac{M(z)}{q(z)(1-q(z))} dz \end{cases}$$

With the choice  $M(s) = s(1-s)$ , we have  $c_M = 1$  and with the choice  $M(s) = s^2(1-s)^2$ , we have  $c_M = \frac{1}{6}$ . A higher order mobility  $M$  will inevitably lower the constant in front of the velocity but will prove to be necessary to find the right motion as stated in Result 2.1.

We start off with the classical Cahn–Hilliard model with non negative mobility  $M$  and potential  $W(s) = \frac{s^2(1-s)^2}{2}$ , that we refer to as **M-CH** from now on:

$$(4) \quad \begin{cases} \varepsilon^2 \partial_t u = \text{div}(M(u)\nabla\mu) \\ \mu = W'(u) - \varepsilon^2 \Delta u \end{cases}$$

When the mobility  $M$  is a scalar positive weight independent of  $u$ , we recall that the equation

$$\begin{cases} \varepsilon^2 \partial_t u = \text{div}(M\nabla\mu) \\ \mu = W'(u) - \varepsilon^2 \Delta u \end{cases}$$

is the  $H^{-1}$  gradient flow of the Cahn–Hilliard energy

$$(5) \quad E(u) = \int_Q \frac{\varepsilon}{2} |\nabla u|^2 + \frac{1}{\varepsilon} W(u) \, dx$$

when considering the following scalar product in  $H_0^1$  weighted by the mobility  $M$ :

$$(6) \quad \langle f, g \rangle_{H_0^1} = \int_Q M \nabla f \cdot \nabla g \, dx.$$

It is important to note that the mobility is incorporated in the metric with respect to which the gradient flow is computed, and not as a geometric parameter in the energy.

Equation (4) is an extension of the above equation to the case where  $M$  depends on  $u$ .

The **M-CH** model has been extensively studied and it is well understood that the mobility needs to be a polynomial of order at least 2. Indeed, a mobility of order 1 would give a quicker motion, but as already mentioned the authors of [31] showed that it yields an additional undesired bulk diffusion term in the limit velocity. This term can be removed the pure surface diffusion motion can be recovered by choosing a higher order mobility, which is what we will do.

**2.2. Properties of the classical Cahn–Hilliard model with mobility.** The properties of **M-CH** are summarized in the following result, see [31]:

**Proposition 2.1.** *With the choice  $M(s) = s^2(1-s)^2$ , the solution  $u_\varepsilon$  to (4) expands formally near the interface  $\Gamma_\varepsilon(t) = \{u_\varepsilon(t, \cdot) = \frac{1}{2}\}$  as:*

$$(7) \quad u_\varepsilon(t) = q \left( \frac{\text{dist}(x, \Omega_\varepsilon(t))}{\varepsilon} \right) + \mathcal{O}(\varepsilon)$$

with  $\Omega_\varepsilon(t) = \{u_\varepsilon(t, \cdot) \leq \frac{1}{2}\}$ . The associated normal velocity satisfies:

$$(8) \quad V = c_W c_M \Delta_\Gamma H + \mathcal{O}(\varepsilon)$$

If we do not require  $M'(0) = M'(1) = 0$ , i.e.  $M$  to be a double well polynomial mobility with roots 0 and 1 of multiplicity at least two, then the velocity contains an additional undesired bulk diffusion term. For example, if we set  $M(s) = s(1-s)$ , then

$$(9) \quad V = c_W c_M \Delta_\Gamma H \pm c_W^2 c_M H \nabla_n H$$

Moreover, the volume is preserved only up to an order  $\mathcal{O}(\varepsilon)$ :

$$(10) \quad |\Omega_\varepsilon(t)| = |\Omega_\varepsilon(0)| + \mathcal{O}(\varepsilon)$$

From now on, we fix the mobility  $M$  to be

$$M(s) = s^2(1-s)^2.$$

**M-CH** has a well identified drawback. The leading error term in (7) is of order  $\varepsilon$  and has a dependence in the curvature. This means it becomes relevant in high curvature regions. This is especially problematic when reaching the pure states because an overshoot due to oscillations occurs, and the solution does not stay within its physical range  $[0, 1]$ . This problem proves to be even more problematic in the multiphase case because the solutions may not be positive anymore and phantom phases may appear.

The volume conservation is a standard property of the Cahn–Hilliard model on a domain  $Q$  with periodic or Neumann homogeneous boundary conditions on  $\partial Q$ :

$$\frac{d}{dt} \int_Q u \, dx = \int_Q \partial_t u \, dx = \int_Q \text{div}(M(u) \nabla \mu) \, dx = 0.$$

However, numerically, the quality of the conservation is constrained by the quality of the approximation of the solution  $u_\varepsilon$ . As we will see with the later models, a more accurate solution  $u_\varepsilon$  will also lead to a more accurate conservation of the volume.

### 3. A NEW VARIATIONAL MODEL WITH TWO MOBILITIES

In this section, we propose a new variational Cahn–Hilliard model with two mobilities. In contrast with [40] where the energy is modified, we propose to incorporate the additional degeneracy in the metric used for defining the gradient flow. First, we derive our model and explain the right choice for its parameters. Then we review its theoretical properties, that appear to be similar as those of the previous model when we choose  $p = 1$ . We compare the numerical behavior of each method in the next section devoted to numerics.

**3.1. Derivation of the model.** Our model derives from the classical Cahn–Hilliard energy:

$$E(u) = \int_Q \frac{\varepsilon}{2} |\nabla u|^2 + \frac{1}{\varepsilon} W(u) \, dx$$

Let us consider a  $H_0^1$  scalar product with two scalar positive weights  $M$  and  $N$ :

$$\langle f, g \rangle_{H_0^1} = \int_Q M \nabla(Nf) \cdot \nabla(Ng) \, dx$$

Taking the  $H^{-1}$  gradient flow of the energy  $E$  with respect to this scalar product, we obtain the following equation:

$$\begin{cases} \varepsilon^2 \partial_t u = N \text{div}(M \nabla(N\mu)) \\ \mu = -\varepsilon^2 \Delta u + W'(u) \end{cases}$$

Considering now a dependence on  $u$  of  $M$  and  $N$  gives the following equation, that we refer to as the **NMN-CH** model:

$$(11) \quad \begin{cases} \varepsilon^2 \partial_t u = N(u) \operatorname{div}(M(u) \nabla(N(u)\mu)) \\ \mu = -\varepsilon^2 \Delta u + W'(u) \end{cases}$$

This model has the advantage of conserving the minimized energy and being variational in the following sense:

$$\begin{aligned} \frac{d}{dt} E(u) &= \int_Q (-\varepsilon \Delta u + W'(u)) \partial_t u dx \\ &= \int_Q N(u) \mu \operatorname{div}(M(u) \nabla(N(u)\mu)) dx \\ &= - \int_Q M(u) |\nabla(N(u)\mu)|^2 dx + \int_{\partial\Omega} M(u) N(u) \mu \nabla(N(u)\mu) \cdot n d\sigma \\ &= - \int_Q M(u) |\nabla(N(u)\mu)|^2 dx \leq 0 \end{aligned}$$

in the case of periodic or Neumann homogeneous boundary conditions on  $\partial Q$ .

**3.2. Choosing  $N$ .** As previously stated,  $M$  is set to be:

$$M(s) = s^2(1-s)^2.$$

We want to choose  $N$  so that it has an antagonist effect to  $M$  and forces the leading error term  $U_1$  to be zero, see below. We will show that the correct choice for  $N$  is:

$$(12) \quad N(s) = \frac{1}{\sqrt{M(s)}} = \frac{1}{s(1-s)}$$

Indeed, the following equation is obtained for  $U_1$  (see details below):

$$\partial_{zz} U_1 - W''(U_0) U_1 = H \partial_z U_0 - \mu_1$$

and with the above choice for  $N$  we have:

$$H \partial_z U_0 = \mu_1$$

Thus  $U_1 = 0$  while other choices for  $N$  only impose  $U_1 \rightarrow 0$  far from the interface.

We define the following integral:

$$c_N = \int_{-\infty}^{+\infty} \frac{q'(z)}{N(q(z))} dz$$

In conclusion, the correct choice for  $N$  is (12).

**3.3. Properties of the NMN-CH model.** They are summarized in the following result, to be compared with Proposition 2.1.

**Proposition 3.1.** *If we choose  $M(s) = s^2(1-s)^2$  and  $N(s) = \frac{1}{\sqrt{M(s)}} = \frac{1}{s(1-s)}$ , the solution  $u_\varepsilon$  to (11) expands formally near the interface  $\Gamma_\varepsilon(t)$  as:*

$$(13) \quad u_\varepsilon = q \left( \frac{\operatorname{dist}(x, \Omega_\varepsilon(t))}{\varepsilon} \right) + \mathcal{O}(\varepsilon^2)$$

with  $\Omega_\varepsilon(t) = \left\{ u_\varepsilon \leq \frac{1}{2} \right\}$ . The associated normal velocity satisfies:

$$(14) \quad V = \frac{c_W c_M}{c_N^2} \Delta_\Gamma H + \mathcal{O}(\varepsilon)$$

Moreover, the volume is preserved up to an order  $\mathcal{O}(\varepsilon^2)$ :

$$(15) \quad |\Omega_\varepsilon(t)| = |\Omega_\varepsilon(0)| + \mathcal{O}(\varepsilon^2)$$

#### 4. PROOF OF PROPOSITION 3.1

In this section we prove Proposition 3.1 which summarizes the properties of **NMN-CH**. We start with the volume conservation (15), assuming the other properties as in [9]. Then, we introduce the tools and notations to derive the formal asymptotics and demonstrate (13) and (14).

**4.1. Proof of the volume conservation.** In this part, we demonstrate (15) when assuming the profile (13), which we will prove in the next part. We recall the following relations linking  $W$  with  $M$  and  $N$ :

$$W(s) = \frac{1}{2}s^2(1-s)^2, \quad M(s) = 2W(s), \quad \text{and} \quad N(s) = \frac{1}{\sqrt{2W(s)}}.$$

The proof is done in two steps. First, we give the expression of the volume in terms of an integral of the function  $G(s) = \int_0^s \sqrt{2W(s)} ds$  and use it to show the volume conservation of the **NMN-CH** model using the form of the profile  $u$  given by (13). Then we show the validity of this expression to conclude the proof.

The formula linking the volume of  $\Omega_\varepsilon(t)$  with  $G$  is the following:

$$(16) \quad |\Omega_\varepsilon(t)| = \int_Q 6(G \circ q) \left( \frac{d(x, \Omega_\varepsilon(t))}{\varepsilon} \right) dx + \mathcal{O}(\varepsilon^2)$$

where  $d$  is the signed distance function to the interface of  $\Omega$  and  $d(x, \Omega) < 0$  for  $x \in \Omega$ .

Under the assumption that the profile  $u_\varepsilon$  is given by:

$$u_\varepsilon(x, t) = q \left( \frac{d(x, \Omega_\varepsilon(t))}{\varepsilon} \right) + \mathcal{O}(\varepsilon^2),$$

we have by composition by  $G$  and integration:

$$\int_{\mathbb{R}^d} G(u_\varepsilon(x, t)) = \int_{\mathbb{R}^d} (G \circ q) \left( \frac{d(x, \Omega_\varepsilon(t))}{\varepsilon} \right) + \mathcal{O}(\varepsilon^2)$$

Using (16), we conclude:

$$\forall t \geq 0, |\Omega_\varepsilon(t)| = \int_{\mathbb{R}^d} G(u_\varepsilon(x, t)) dx + \mathcal{O}(\varepsilon^2)$$

Considering periodic or Neumann boundary condition on  $Q$  leads to a conservation of the integral of  $G$  along the time:

$$\begin{aligned} \frac{d}{dt} \int_Q G(u_\varepsilon) &= \int_Q G'(u_\varepsilon) \partial_t u_\varepsilon \\ &= \frac{1}{\varepsilon^2} \int_Q \left( \sqrt{2W(u_\varepsilon)} N(u_\varepsilon) \right) \operatorname{div} (M(u_\varepsilon) \nabla (N(u_\varepsilon) \mu)) \\ &= \frac{1}{\varepsilon^2} \int_Q \operatorname{div} (M(u_\varepsilon) \nabla (N(u_\varepsilon) \mu)) \\ &= \frac{1}{\varepsilon^2} \int_{\partial Q} M(u_\varepsilon) \nabla (N(u_\varepsilon) \mu) \cdot n = 0 \end{aligned}$$

This means that the volume is conserved over time and (15) is verified if (16) is satisfied.

We now turn to the proof of (16). For the simplicity of the notations of the bounds of the integrals, we work in  $\mathbb{R}^d$ , but the result remains true for any regular bounded domain  $Q$ . Using the coarea formula, we have:

$$\int_{\mathbb{R}^d} 6(G \circ q) \left( \frac{d(x, \Omega_\varepsilon(t))}{\varepsilon} \right) = 6 \int_{\mathbb{R}} h(s) G \left( q \left( \frac{s}{\varepsilon} \right) \right) ds$$

where  $h(s) = |D\chi_{\{d(x, \Omega_\varepsilon(t)) \leq s\}}|$  is the perimeter of the signed distance function to  $\Omega_\varepsilon(t)$ . Using the fact that:

$$6G(q(-s)) = 6G(1 - q(s)) = 1 - 6G(q(s))$$

We deduce:

$$\begin{aligned}
\int_{\mathbb{R}^d} 6(G \circ q) \left( \frac{d(x, \Omega_\varepsilon(t))}{\varepsilon} \right) &= \int_{-\infty}^0 h(s) + \int h(s) \left( 6G \left( q \left( \frac{s}{\varepsilon} \right) \right) - 1 \right) + 6 \int_0^{+\infty} h(s) G \left( q \left( \frac{s}{\varepsilon} \right) \right) dx \\
&= |\Omega_\varepsilon(t)| - \int_{-\infty}^0 h(s) G \left( q \left( \frac{-s}{\varepsilon} \right) \right) + 6 \int_0^{+\infty} h(s) G \left( q \left( \frac{s}{\varepsilon} \right) \right) dx \\
&= |\Omega_\varepsilon(t)| + 6\varepsilon \int_0^{+\infty} [h(\varepsilon s) - h(-\varepsilon s)] G(q(s)) ds
\end{aligned}$$

Equation (16) is verified if we manage to show that the second term of the right hand side is  $\mathcal{O}(\varepsilon^2)$ . Using the regularity of  $\Omega_\varepsilon(t)$ , we have:

$$\forall s \in ]0, |\log(\varepsilon)|[ \quad h(\varepsilon s) - h(-\varepsilon s) = 2\varepsilon h'(0) + \mathcal{O}(s^2 \varepsilon^2)$$

As  $q(s) = \frac{1 - \tanh(s)}{2}$  and  $G$  is an increasing polynomial function, the moments  $\int_0^{+\infty} s^n q(s) ds$  are finite. Then,

$$\begin{aligned}
\left| \int_0^{|\log(\varepsilon)|} (h(\varepsilon s) - h(-\varepsilon s)) G(q(s)) ds \right| &\leq \left| \int_0^{|\log(\varepsilon)|} (2s\varepsilon h'(0) + Cs^2 \varepsilon^2) G(q(s)) ds \right| \\
&= \mathcal{O}(\varepsilon)
\end{aligned}$$

On the other hand, we know that  $h(s) \sim_{s \rightarrow +\infty} s^{d-1}$ :

$$\int_{|\log(\varepsilon)|}^{+\infty} h(\varepsilon s) G(q(s)) ds \leq C\varepsilon^{d-1} \int_{|\log(\varepsilon)|}^{+\infty} s^{d-1} G(q(s)) ds = \mathcal{O}(\varepsilon^{d-1})$$

and that  $h$  is bounded in  $\mathbb{R}_-^*$ :

$$\int_{|\log(\varepsilon)|}^{+\infty} h(-\varepsilon s) G(q(s)) ds \leq C \int_{|\log(\varepsilon)|}^{+\infty} G(q(s)) ds = \mathcal{O}(\varepsilon)$$

Globally, we conclude that:

$$6\varepsilon \int_0^{+\infty} [h(\varepsilon s) - h(-\varepsilon s)] G(q(s)) ds = \mathcal{O}(\varepsilon^2)$$

and that (16) is true and the property (15) is established under the condition that (13) is verified. This is the object of the next part of this section.

**4.2. Formal asymptotics toolbox.** Before the actual computations, we first recall the tools necessary to derive our formal asymptotic derivation, following the notations of [2, 19, 12] and the results in differential geometry of [4]. The principle is to study separately the behavior of the solution near the interface and far from it. We will do the derivations in dimension 2 for the sake of simplicity of the notations and readability, but the principle is identical in higher dimension.

To derive the method we require that the interface  $\Gamma(t, \varepsilon)$  remains smooth enough and that there exists a neighbourhood  $\mathcal{N} = \mathcal{N}_\delta(\Gamma(t, \varepsilon)) = \{x \in \Omega / |(x, t) < 3\delta\}$  in which the signed distance function  $d$  is well-defined.  $\mathcal{N}$  is called the *inner region* near the interface and its complementary the *outer region*.

**Outer variables:** Far from the interface, we consider the *outer functions*  $(u, \mu)$  depending on the standard *outer variable*  $x$ . The system remains the same:

$$(17) \quad \begin{cases} \varepsilon^2 \partial_t u = N(u) \operatorname{div}(M(u) \nabla(N(u) \mu)) \\ \mu = -\varepsilon^2 \Delta u + W'(u) \end{cases}$$



**Inner variables:** Inside  $\mathcal{N}$ , we define the *inner functions*  $(U, \boldsymbol{\mu})$  depending on the *inner variables*  $(z, s)$ , where  $z$  is the variable along the normal and  $s$  is the variable in the direction of the arc-length parametrization  $S$  of the interface  $\Gamma$ :

$$\begin{cases} U(z, s, t) := U\left(\frac{d(x, t)}{\varepsilon}, S(x, t), t\right) = u(x, t) \\ \boldsymbol{\mu}(z, s, t) := \boldsymbol{\mu}\left(\frac{d(x, t)}{\varepsilon}, S(x, t), t\right) = \boldsymbol{\mu}(x, t) \end{cases}$$

In order to express the derivatives of  $U$ , we first need to calculate the gradient and the laplacian of  $d$  and  $S$ . The properties of  $d$  are common knowledge in differential geometry, see for instance [4]:

$$\begin{cases} \nabla d(x, t) = n(x, t) \\ \Delta d(x, t) = \sum_{k=1}^{d-1} \frac{\kappa_k(\pi(x))}{1 + \kappa_k(\pi(x))d(x, t)} \\ \quad = \frac{H}{1 + \varepsilon z H} \text{ in dimension 2} \end{cases}$$

Let  $X_0(s, t)$  be a given point of the interface, then deriving the equation connecting the variable  $s$  and the function  $S$  gives:

$$s = S(X_0(s, t) + \varepsilon z n(s, t), t)$$

with respect to  $z$ :

$$\begin{aligned} 0 &= \varepsilon n \cdot \nabla S \\ &= \varepsilon \nabla d \cdot \nabla S \end{aligned}$$

This means that there are no cross derivative terms. We now derive the same equation with respect to  $s$ :

$$\begin{aligned} 1 &= (\partial_s X_0 + \varepsilon z H \partial_s n) \cdot \nabla S \\ &= (1 + \varepsilon z H) \tau \cdot \nabla S \end{aligned}$$

We know that  $\nabla S$  is orthogonal to  $n$ , meaning it is colinear to the tangent  $\tau$ , then:

$$\nabla S = \frac{1}{1 + \varepsilon z H} \tau$$

Taking the divergence, we find  $\Delta S$ :

$$\begin{aligned} \Delta S &= \operatorname{div}\left(\frac{1}{1 + \varepsilon z H} \tau\right) \\ &= \nabla\left(\frac{1}{1 + \varepsilon z H}\right) \cdot \tau + \frac{1}{1 + \varepsilon z H} \operatorname{div}(\tau) \\ &= \frac{1}{1 + \varepsilon z H} \partial_s \left(\frac{1}{1 + \varepsilon z H}\right) + \frac{1}{1 + \varepsilon z H} \tau \cdot \partial_s \tau \\ &= -\frac{\varepsilon z \partial_s H}{(1 + \varepsilon z H)^3} \end{aligned}$$

To express the connection between the derivatives of  $U, \boldsymbol{\mu}$  and  $u, \boldsymbol{\mu}$ , we come back to the definition of the inner functions:

$$(18) \quad u(x, t) = U\left(\frac{d(x, t)}{\varepsilon}, S(x, t), t\right)$$

Successive derivations with respect to  $x$  give the following equations

$$(19) \quad \begin{cases} \nabla u = \nabla d \frac{1}{\varepsilon} \partial_z U + \nabla S \partial_s U \\ \Delta u = \Delta d \frac{1}{\varepsilon} \partial_z U + \frac{1}{\varepsilon^2} \partial_{zz} U + \Delta S \partial_s U + |\nabla S|^2 \partial_{ss} U \\ \operatorname{div}(M(u) \nabla(N(u) \mu)) = \frac{1}{\varepsilon^2} (\partial_z M \partial_z(N \mu)) + \frac{M}{\varepsilon} \Delta d \partial_z(N \mu) \\ \quad + |\nabla S|^2 \partial_s(M \partial_s(N \mu)) + \Delta S M \partial_s(N \mu) \end{cases}$$

The *inner system* of the **NMN-CH** model finally reads:

$$(20) \quad \begin{cases} \varepsilon^2 \partial_t U + \varepsilon^2 \partial_t S \partial_s U - \varepsilon V \partial_z U = \frac{N}{\varepsilon^2} \partial_z (M \partial_z(N \mu)) + \frac{NM}{\varepsilon} \Delta d \partial_z(N \mu) + T_1(s) \\ \mu = W'(U) - \partial_{zz} U - \varepsilon \Delta d \partial_z U - \varepsilon^2 T_2(s) \\ T_1(s) = -\frac{\varepsilon z \partial_s H N M}{(1 + \varepsilon z H)^3} \partial_s(N \mu) + \frac{N}{(1 + \varepsilon z H)^2} \partial_s(M \partial_s(N \mu)) \\ T_2(s) = -\frac{\varepsilon z \partial_s H}{(1 + \varepsilon z H)^3} \partial_s U + \frac{1}{(1 + \varepsilon z H)^2} \partial_{ss} U \\ \Delta d = \frac{H}{1 + \varepsilon z H} \end{cases}$$

**Independence in  $z$  of the normal velocity  $V$ :** The normal velocity of the interface  $V(s, t)$  is defined by:

$$V(s, t) = \partial_t X_0(s, t) \cdot n(s, t)$$

In the neighbourhood  $\mathcal{N}$ , we have the following property (which is a direct consequence of the definition of the signed distance function):

$$d(X_0(s, t) + \varepsilon z n(s, t), t) = \varepsilon z$$

Deriving this with respect to  $t$  yields:

$$V(s, t) = \partial_t X_0(s, t) \cdot \nabla d(X_0(s, t) + \varepsilon z n(s, t), t) = -\partial_t d(X(z, s, t), t)$$

Thus, the function  $\partial_t d(x, t)$  is independent of  $z$  and we can extend the function everywhere in the neighbourhood by choosing:

$$V(X_0(s, t) + \varepsilon z n, t) := -\partial_t d(X_0(s, t) + \varepsilon z n, t) = V(s, t)$$

This property of independence is crucial to be able to extract the velocity from integrals in  $z$  in the following derivations.

**Taylor expansions:** We assume the following Taylor expansions for our functions:

$$\begin{aligned} u(x, t) &= u_0(x, t) + \varepsilon u_1(x, t) + \varepsilon^2 u_2(x, t) + \dots \\ U(z, s, t) &= U_0(z, s, t) + \varepsilon U_1(z, s, t) + \varepsilon^2 U_2(z, s, t) + \dots \\ \mu(x, t) &= \mu_0(x, t) + \varepsilon \mu_1(x, t) + \varepsilon^2 \mu_2(x, t) + \dots \\ \mu(z, s, t) &= \mu_0(z, s, t) + \varepsilon \mu_1(z, s, t) + \varepsilon^2 \mu_2(z, s, t) + \dots \end{aligned}$$

We can then compose these expansions with a regular function  $F$ :

$$\begin{aligned} F(U) &= F(U_0) + \\ &\quad + \varepsilon F'(U_0) U_1 + \\ &\quad + \varepsilon^2 \left[ F'(U_0) U_2 + \frac{F''(U_0)}{2} U_1^2 \right] + \\ &\quad + \varepsilon^3 \left[ F'(U_0) U_3 + F''(U_0) U_1 U_2 + \frac{F'''(U_0)}{6} U_1^3 \right] + \dots \end{aligned}$$

We can now investigate order by order the behavior of the system. We have to study four orders as the velocity appears in the fourth order of the first equation of the Cahn–Hilliard system.

To simplify the notation within the asymptotics, we adopt the following notations for  $M(u)$ :

$$M(u) = m_0 + \varepsilon m_1 + \varepsilon^2 m_2 + \dots ,$$

where each term corresponds to:

$$\begin{cases} m_0 = M(u_0) \\ m_1 = M'(u_0)u_1 \\ m_2 = M'(u_0)u_2 + \frac{M''(u_0)}{2}(u_1)^2 \end{cases}$$

We adopt the same convention for any generic *outer function*  $F(u)$  or *inner function*  $F(U)$ :

$$\begin{aligned} F(u) &= f_0 + \varepsilon f_1 + \varepsilon^2 f_2 + \varepsilon^3 f_3 + \dots \\ F(U) &= F_0 + \varepsilon F_1 + \varepsilon^2 F_2 + \varepsilon^3 F_3 + \dots \end{aligned}$$

We can now investigate order by order the behavior of system (11). We have to study up to the fourth order where the leading order of the velocity will appear in the first equation of (17).

**Flux matching condition between inner and outer equations:** Instead of using the matching conditions directly between the first equations of the inner and outer systems, it is more convenient to perform the matching on the flux  $j = M(u)\nabla(\sigma\mu + \lambda)$ . It has the following Taylor expansion:

$$\begin{aligned} (21) \quad j &= [m_0\nabla(n\mu)_0] \\ &+ \varepsilon [m_1\nabla(n\mu)_0 + m_0\nabla(n\mu)_1] \\ &+ \varepsilon^2 [m_2\nabla(n\mu)_0 + m_1\nabla(n\mu)_1 + m_0\nabla(n\mu)_2] \\ &+ \mathcal{O}(\varepsilon^3) \end{aligned}$$

In inner coordinates, we only need to express the normal part  $J_n := J \cdot n = \frac{M(U)}{\varepsilon}\partial_z\boldsymbol{\mu}$  because the tangential part terms are of higher order. It expands as:

$$\begin{aligned} (22) \quad J_n &= \frac{1}{\varepsilon} [M_0\partial_z(N\boldsymbol{\mu})_0] \\ &+ [M_1\partial_z(N\boldsymbol{\mu})_0 + M_0\partial_z(N\boldsymbol{\mu})_1] \\ &+ \varepsilon [M_2\partial_z(N\boldsymbol{\mu})_0 + M_1\partial_z(N\boldsymbol{\mu})_1 + M_0\partial_z(N\boldsymbol{\mu})_2] \\ &+ \varepsilon^2 [M_3\partial_z(N\boldsymbol{\mu})_0 + M_2\partial_z(N\boldsymbol{\mu})_1 \\ &\quad + M_1\partial_z(N\boldsymbol{\mu})_2 + M_0\partial_z(N\boldsymbol{\mu})_3] \\ &+ \mathcal{O}(\varepsilon^3) \end{aligned}$$

The flux matching conditions allow to match the limit as  $z \rightarrow \pm\infty$  of terms of (21) with the correspond order terms of (22).

**4.3. Formal matched asymptotic analysis for the new NMN-CH model.** Now that all the tools necessary are defined, we start the derivation of the proof of Proposition 3.1. At first order, we determine the profile of the solution. At second order, we link the curvature with the leading term of  $\boldsymbol{\mu}$  and prove that the leading error term is zero. The third order is used to establish certain relations between different terms and finally we recover the velocity in the fourth order.

**First order:** At order  $(\mathcal{O}(1), \mathcal{O}(1))$  the outer system (17) reads:

$$(23) \quad \begin{cases} 0 = N_0 \operatorname{div}(M_0 \nabla(N_0 \mu_0)) \\ \mu_0 = W'(u_0) \end{cases}$$

At order  $(\mathcal{O}(\varepsilon^{-2}), \mathcal{O}(1))$  the inner system (20) reads:

$$\begin{cases} 0 = N_0 \partial_z (M_0 \partial_z (N_0 \mu_0)) \\ \mu_0 = W'(U_0) - \partial_{zz} U_0 \end{cases}$$

The first equation gives that  $M_0 \partial_z (N_0 \mu_0) = B_0$  is constant in  $z$ . The matching conditions on the outer flux (21) and the inner flux (22) at order  $\varepsilon^{-1}$  impose this constant to be zero. Then  $N_0 \mu_0$  is constant. The matching conditions with the outer system (23) give that:

$$\mu_0 = 0$$

Then  $U_0$  satisfies the differential equation:

$$\partial_{zz} U_0 - W'(U_0) = 0$$

The solution to this equation is the profile  $q$  given by (3). Thus the first order results in:

$$\begin{cases} \mu_0 = 0 \\ U_0 = q(z) := \frac{1 - \tanh(\frac{z}{2})}{2} \end{cases}$$

**Second order:** At order  $(\mathcal{O}(\varepsilon), \mathcal{O}(\varepsilon))$  the outer system (17) reads:

$$(24) \quad \begin{cases} 0 = N_0 \operatorname{div}(M_0 \nabla(N_0 \mu_1)) \\ \mu_1 = W''(u_0) u_1 = u_1 \end{cases}$$

At order  $(\mathcal{O}(\varepsilon^{-1}), \mathcal{O}(\varepsilon))$  the inner system (20) reads:

$$(25) \quad \begin{cases} 0 = N_0 \partial_z (M_0 \partial_z (N_0 \mu_1)) \\ \mu_1 = W''(U_0) U_1 - \partial_{zz} U_1 - H \partial_z U_0 \end{cases}$$

The first equation of (25) shows that  $N_0 \mu_1$  is a certain constant  $B_1$ . The matching conditions between the inner flux (22) and the outer flux (21) at order 0 require that (by removing all null terms):

$$B_1 = \lim_{z \rightarrow +\infty} M_0 \partial_z (N_0 \mu_1) = 0$$

Then there exists a function  $A_1$  constant in  $z$  such that  $N_0 \mu_1 = A_1$ . The matching from inner to outer for  $\mu$  yields:

$$\mu_1 = \lim_{z \rightarrow \pm\infty} \mu_1 = \lim_{z \rightarrow \pm\infty} \frac{A_1}{N_0} = 0$$

From the matching conditions with the second equation of (24) we have:

$$u_1 = \mu_1 = 0$$

We now determine the value of  $A_1$  using the second equation of (25). We multiply it by  $\partial_z U_0$  and integrate it. We divide the equation in three terms. The left hand side term gives:

$$\int \mu_1 \partial_z U_0 = \int N_0 \mu_1 \frac{\partial_z U_0}{N_0} = A_1 \int_{-\infty}^{+\infty} \frac{\partial_z U_0(z)}{N(U_0(z))} dz = A_1 c_N$$

The first two terms in the right hand side vanish:

$$\begin{aligned} \int W''(U_0) U_1 \partial_z U_0 - \partial_{zz} U_1 \partial_z U_0 &= \int \partial_z (W'(U_0)) U_1 - \partial_{zz} U_1 \partial_z U_0 \\ &= - \int \underbrace{(W'(U_0) - \partial_{zz} U_0)}_{=0} \partial_z U_1 \\ &\quad + [W'(U_0) U_1 - \partial_z U_0 \partial_z U_1]_{-\infty}^{+\infty} \\ &= 0 \end{aligned}$$

The fact that the functions in the bracket term vanishes at the limit  $z \rightarrow \pm\infty$  comes from the matching conditions. The second right hand side term results in the curvature:

$$\int -H(\partial_z U_0)^2 dz = -H \int_{-\infty}^{+\infty} q'(z)^2 dz = -c_W H$$

Then:

$$(26) \quad N_0 \boldsymbol{\mu}_1 = A_1 = -\frac{c_W}{c_N} H$$

In conclusion, we have the following properties:

$$\begin{cases} \boldsymbol{\mu}_1 = -\frac{c_W}{c_N} \frac{H}{N(q)} \\ \partial_{zz} U_1 - W''(U_0) U_1 = H q'(z) - \boldsymbol{\mu}_1 \\ \mu_1 = u_1 = 0 \end{cases}$$

Reminding that  $N(z) = -\frac{1}{q'(z)}$ , the equation verified by  $U_1$  is:

$$\partial_{zz} U_1 - W''(U_0) U_1 = 0$$

To solve this equation, we use the following Lemma, which is now rather standard, see for example [3, 2]:

**Lemma 4.1.** *Let  $A(z)$  be a bounded function on  $-\infty < z < \infty$ . Then the problem:*

$$\begin{cases} \partial_{zz} \psi - W''(q(z)) \psi = A(z) \\ \psi(0) = 0, \quad \psi \in L^\infty(\mathbb{R}) \end{cases}$$

has a solution if and only if:

$$(27) \quad \int_{-\infty}^{+\infty} A(z) q'(z) dz = 0$$

Moreover the solution, if it exists, is unique, satisfies:

$$(28) \quad \forall z \in \mathbb{R}, |\psi(z)| \leq C \|A\|_{L^\infty}$$

and is given by the formula:

$$(29) \quad \psi(z) = q'(z) \int_0^z \left( \frac{1}{(q'(s))^2} \int_{-\infty}^s A(\sigma) q'(\sigma) d\sigma \right) ds$$

**Sketch of the proof:** Multiplying the equation by  $q'$  and integrating by parts, we see that condition (27) is necessary. Reciprocally, if the condition (27) is verified, we can perform the method of variation of constants to find the solution explicitly (29).  $\square$

Using Lemma 4.1 with  $A = 0$ , we have that  $U_1 = 0$ . Therefore the leading error term in  $U$  is of magnitude  $\varepsilon^2$  and (13) of Result (3.1) is verified.

**Third order:** At order  $(\mathcal{O}(\varepsilon^2), \mathcal{O}(\varepsilon^2))$  the outer system (17) reads:

$$(30) \quad \begin{cases} 0 = n_0 \operatorname{div} (m_0 \nabla (n_0 \mu_2 + n_1 \mu_1)) \\ \mu_2 = W'''(u_0) \frac{(u_1)^2}{2} + W''(u_0) u_2 - \Delta u_0 = u_2 \end{cases}$$

At order  $(\mathcal{O}(1), \mathcal{O}(\varepsilon^2))$  the inner system (20) reads:

$$(31) \quad \begin{cases} 0 = N_0 \partial_z (M_0 \partial_z (N_0 \boldsymbol{\mu}_2 + N_1 \boldsymbol{\mu}_1)) \\ \boldsymbol{\mu}_2 = W'''(U_0) \frac{(U_1)^2}{2} + W'(U_0) U_2 - \partial_{zz} U_2 - H \partial_z U_1 + z H^2 \partial_z U_0 \end{cases}$$

Similarly to previous orders, there exists a constant  $B_2$  in  $z$  so that:

$$M_0 \partial_z (N_0 \boldsymbol{\mu}_2 + N_1 \boldsymbol{\mu}_1) = B_2$$

The matching of the flux terms from (21) and (22) of order  $\varepsilon$  (removing all the null terms) yields:

$$B_2 = \lim_{z \rightarrow \pm\infty} M_0 \partial_z (N_0 \boldsymbol{\mu}_2 + N_1 \boldsymbol{\mu}_1) = 0$$

Thus:

$$(32) \quad N_0 \boldsymbol{\mu}_2 + N_1 \boldsymbol{\mu}_1 = A_2$$

The derivative in  $z$  of this term would have appeared at the next order. Now that we know it is constant, we can omit it in the next paragraph.

**Fourth order:** At order  $(\mathcal{O}(\varepsilon^3), \mathcal{O}(\varepsilon^3))$  the outer system (17) reads:

$$(33) \quad \begin{cases} 0 = n_0 \operatorname{div} (n_0 \nabla (n_2 \mu_1 + n_1 \mu_2 + n_0 \mu_3)) \\ \mu_3 = W''(u_0) u_3 + W'''(u_0) u_1 u_2 + \frac{W''''(u_0)}{6} (u_1)^3 - \Delta u_1 \end{cases}$$

At order  $(\mathcal{O}(\varepsilon), \mathcal{O}(\varepsilon^3))$  the inner system (20) reads:

$$(34) \quad \begin{cases} -V_0 \partial_z U_0 = N_0 \partial_z (M_0 \partial_z (N_2 \boldsymbol{\mu}_1 + N_1 \boldsymbol{\mu}_2 + N_0 \boldsymbol{\mu}_3)) + N_0 \partial_s (M_0 \partial_s (N_0 \boldsymbol{\mu}_1)) \\ \boldsymbol{\mu}_3 = W''(U_0) U_3 + W'''(U_0) U_1 U_2 + \frac{W''''(U_0)}{6} (U_1)^3 - \partial_{zz} U_1 \\ -H^3 z^2 \partial_z U_0 + z H^2 \partial_z U_1 - H \partial_z U_2 - \partial_{ss} \boldsymbol{\mu}_1 \end{cases}$$

We determine the velocity  $V_0$  by multiplying by  $\frac{1}{N_0}$  and integrating the first equation of (34). We divide the equality in three terms. The left hand side term isolates the velocity:

$$-V_0 \int \partial_z \frac{U_0}{N(U_0)} = -c_N V_0$$

The first term of the right hand side is a pure derivative:

$$\int \partial_z (M_0 \partial_z (N_2 \boldsymbol{\mu}_1 + N_1 \boldsymbol{\mu}_2 + N_0 \boldsymbol{\mu}_3))$$

Then, by using the matching conditions between the fluxes (22) and (21) at order  $\varepsilon^2$  (the equations (32) and (26) ensuring that the other inner terms are zero) and the fact that  $M$  goes to 0 faster than the terms in  $N$  goes to infinite, we have:

$$[M_0 \partial_z (N_2 \boldsymbol{\mu}_1 + N_1 \boldsymbol{\mu}_2 + N_0 \boldsymbol{\mu}_3)]_{-\infty}^{+\infty} = 0$$

Finally, using (26), the second term of the right hand side gives the surface diffusion part:

$$\int M_0 \partial_{ss} (N_0 \boldsymbol{\mu}_1) = -\frac{c_M c_W}{c_N} \partial_{ss} H$$

In conclusion, we obtain the desired motion (14):

$$V_0 = \frac{c_M c_W}{(c_N)^2} \partial_{ss} H$$

This concludes the proof of Proposition 3.1. □

## 5. NUMERICS: DISCRETIZATION AND EXPERIMENTS

In this section, we propose a generic numerical scheme to solve the three different Cahn–Hilliard models:

- The classical Cahn–Hilliard equation (**C-CH**)

$$\begin{cases} \partial_t u &= \Delta \mu \\ \mu &= \frac{1}{\varepsilon^2} W'(u) - \Delta u, \end{cases}$$

where  $W(s) = \frac{1}{2} s^2 (1-s)^2$ .

- The Cahn–Hilliard model with classical mobility (**M-CH**)

$$\begin{cases} \partial_t u &= \operatorname{div}(M(u)\nabla\mu) \\ \mu &= \frac{1}{\epsilon^2}W'(u) - \Delta u. \end{cases}$$

where the mobility is defined as  $M(u) = c_N^2 2W(u)$ . Here, the constant  $c_N = 6$  is added to get the same limit law as using our new Cahn–Hilliard model.

- New second order variational Cahn–Hilliard equation: (**NMN-CH**)

$$\begin{cases} \partial_t u &= N(u) \operatorname{div}(M(u)\nabla(N(u)\mu)) \\ \mu &= \frac{1}{\epsilon^2}W'(u) - \Delta u \end{cases}$$

where the mobility is defined as  $M(u) = W(u) + \gamma\epsilon^2$  and  $N(u) = \sqrt{M(u)}$ . Here  $\gamma > 0$  is a smoothing parameter and we take  $\gamma = 1$  for all numerical experiments presented below,

Our numerical algorithm is constructed as a semi-implicit Fourier spectral method in the spirit of [18, 9, 11, 13, 10], see [24] for a recent review of numerical methods for the phase field approximation of various geometric flows.

All schemes proposed here are based on a convex splitting of the Cahn–Hilliard energy, which was first proposed by Eyre [27] and became popular as a simple, efficient, and stable scheme to approximate various evolution problems with a gradient flow structure [20, 43, 28, 26, 41, 42]. More recently, a first- and second-order splitting scheme was proposed in [5, 40, 39] to address the case of the Cahn–Hilliard equation with mobility. However, these approaches are based on the finite element method and are not compatible with a Fourier spectral discretization.

In this paper, we therefore propose to generalize the idea of convex splitting using an additionally convex splitting of the variational metric associated to the mobility. The advantage is to make it a very simple and efficient scheme, even in the case of highly contrasted and degenerate mobilities. As an illustration, we present above a numerical implementation of our scheme in **Matlab** that requires less than 40 lines.

In this section, we then give some details about these schemes and propose a numerical comparison of phase field models in space dimensions 2 and 3.

**5.1. Spatial discretization: a Fourier-spectral approach.** All equations are solved on a square-box  $Q = [0, L_1] \times \cdots \times [0, L_d]$  with periodic boundary conditions. We recall that the Fourier  $\mathbf{K}$ -approximation of a function  $u$  defined in a box  $Q = [0, L_1] \times \cdots \times [0, L_d]$  is given by

$$u^{\mathbf{K}}(x) = \sum_{\mathbf{k} \in K_N} c_{\mathbf{k}} e^{2i\pi \xi_{\mathbf{k}} \cdot x},$$

where  $K_N = [-\frac{N_1}{2}, \frac{N_1}{2} - 1] \times [-\frac{N_2}{2}, \frac{N_2}{2} - 1] \cdots \times [-\frac{N_d}{2}, \frac{N_d}{2} - 1]$ ,  $\mathbf{k} = (k_1, \dots, k_d)$  and  $\xi_{\mathbf{k}} = (k_1/L_1, \dots, k_d/L_d)$ . In this formula, the  $c_{\mathbf{k}}$ 's denote the  $K^d$  first discrete Fourier coefficients of  $u$ . The inverse discrete Fourier transform leads to  $u_{\mathbf{k}}^K = \text{IFFT}[c_{\mathbf{k}}]$  where  $u_{\mathbf{k}}^K$  denotes the value of  $u$  at the points  $x_{\mathbf{k}} = (k_1 h_1, \dots, k_d h_d)$  and where  $h_{\alpha} = L_{\alpha}/N_{\alpha}$  for  $\alpha \in \{1, \dots, d\}$ . Conversely,  $c_{\mathbf{k}}$  can be computed as the discrete Fourier transform of  $u_{\mathbf{k}}^K$ , *i.e.*,  $c_{\mathbf{k}} = \text{FFT}[u_{\mathbf{k}}^K]$ .

**5.2. Time discretization.** Given a time discretization parameter  $\delta_t > 0$ , we construct a sequence  $(u^n)_{n \geq 0}$  of approximations of  $u$  at times  $n\delta_t$ .

**5.2.1. An IMEX scheme for the C-CH model.** We propose now to use a simple scheme to discretize the classical Cahn–Hilliard equation

$$\begin{cases} \partial_t u &= \Delta \mu \\ \mu &= \nabla_u E(u) = \frac{1}{\epsilon^2}W'(u) - \Delta u, \end{cases}$$

where the Cahn–Hilliard energy reads as

$$E(u) = \int_Q \varepsilon \frac{|\nabla u|^2}{2} + \frac{1}{\varepsilon} W(u) dx.$$

**A semi-implicit scheme based on a convex-concave splitting of  $E$ :** Following the idea of [27], we propose to split the energy  $E$  as the sum of a convex energy and a concave energy

$$E(u) = E_c(u) + E_e(u),$$

with, respectively, an implicit and an explicit integration of the convex and concave parts:

$$\begin{cases} (u^{n+1} - u^n)/\delta_t & = \Delta \mu^{n+1} \\ \mu^{n+1} & = \nabla_u E_c(u^{n+1}) + \nabla_u E_e(u^n) \end{cases}$$

Notice that this scheme can also be interpreted as an implicit discretization of the semi linearized PDE

$$\begin{cases} \partial_t u & = \Delta \mu \\ \mu & = \nabla_u \bar{E}_{u^n}(u) = \nabla_u E_c(u) + \nabla_u E_e(u^n) \end{cases},$$

where the new associated energy  $\bar{E}_{u^n}$  reads as

$$\bar{E}_{u^n}(u) = E_c(u) + E_e(u^n) + \langle \nabla_u E_e(u^n), (u - u^n) \rangle.$$

This continuous point of view shows that  $\bar{E}_{u^n}(u)$  is clearly decreasing along the flow

$$\frac{d}{dt} \left( \bar{E}_{u^n}(u) \right) = \langle \bar{E}_{u^n}(u), u_t \rangle = -\|\nabla \bar{E}_{u^n}(u)\|^2 < 0.$$

and then

$$\bar{E}_{u^n}(u^{n+1}) \leq \bar{E}_{u^n}(u^n) = E(u^n),$$

Finally, the assumption on the concavity of  $E_e$  implies that  $E(u) \leq \bar{E}_{u^n}(u)$  and gives the decreasing of  $E$ ,

$$E(u^{n+1}) \leq E(u^n).$$

without requiring any assumption on the time step  $\delta_t$ .

**Application in the case of the Cahn–Hilliard energy:** In the case of the Cahn–Hilliard equation using the smooth double well potential  $W(s) = \frac{1}{2}s^2(1-s)^2$ , a standard splitting choice is

$$E_c(u) = \frac{1}{2} \int_Q \varepsilon |\nabla u|^2 + \frac{\alpha}{\varepsilon^2} u^2 dx \text{ and } E_e(u) = \int_Q \frac{1}{\varepsilon} (W(u) - \alpha \frac{u^2}{2}) dx.$$

Notice that  $E_e$  is clearly concave as soon as  $\alpha \geq \max_{s \in [0,1]} |W''(s)|$ . In particular, this approach leads to the semi-implicit scheme

$$\begin{cases} (u^{n+1} - u^n)/\delta_t & = \Delta \mu^{n+1} \\ \mu^{n+1} & = \left( -\Delta u^{n+1} + \frac{\alpha}{\varepsilon^2} u^{n+1} \right) + \left( \frac{1}{\varepsilon^2} (W'(u^n) - \alpha u^n) \right), \end{cases}$$

which also reads as

$$\begin{pmatrix} I_d & -\delta_t \Delta \\ \Delta - \alpha/\varepsilon^2 & I_d \end{pmatrix} \begin{pmatrix} u^{n+1} \\ \mu^{n+1} \end{pmatrix} = \begin{pmatrix} u^n \\ \frac{1}{\varepsilon^2} (W'(u^n) - \alpha u^n) \end{pmatrix}.$$

Finally, the couple  $(u^{n+1}, \mu^{n+1})$  can be expressed as

$$u^{n+1} = L \left[ u^n + \frac{\delta_t}{\varepsilon^2} \Delta (W'(u^n) - \alpha u^n) \right] \text{ and } \mu^{n+1} = L \left[ \frac{1}{\varepsilon^2} (W'(u^n) - \alpha u^n) \right].$$

Here, the operator  $L = (I_d + \delta_t \Delta (\Delta - \alpha/\varepsilon^2 I_d))^{-1}$  can be easily computed in Fourier space like a symbol operator associated to

$$\hat{L}(\xi) = 1/(1 + \delta_t 4\pi^2 |\xi|^2 (4\pi^2 |\xi|^2 + \alpha/\varepsilon^2)).$$



5.2.2. *A numerical scheme for the M-CH model.* We now consider the case of the **M-CH** model, which reads

$$\begin{cases} \partial_t u &= \operatorname{div}(M(u)\nabla\mu) \\ \mu &= \frac{1}{\epsilon^2}W'(u) - \Delta u. \end{cases}$$

As previously, it should be interesting to consider the following scheme

$$\begin{cases} (u^{n+1} - u^n)/\delta_t &= \operatorname{div}(M(u^n)\nabla\mu^{n+1}) \\ \mu^{n+1} &= \nabla_u E_c(u^{n+1}) + \nabla_u E_e(u^n). \end{cases}$$

It can also be interpreted as an implicit discretization of the modified Cahn–Hilliard system

$$\begin{cases} \partial_t u &= \operatorname{div}(M(u^n)\nabla\mu) \\ \mu &= \nabla_u \bar{E}_{u^n}, \end{cases}$$

which shows that  $E(u^{n+1}) \leq E(u^n)$  as

$$\frac{d}{dt} \left( \bar{E}_{u^n}(u) \right) = \langle \bar{E}_{u^n}(u), u_t \rangle = -\|\sqrt{M(u^n)}\nabla\bar{E}_{u^n}(u)\|^2 < 0.$$

However, such an approach requires the computation of the new operator  $L_{M,u^n}$  defined by  $L_{M,u^n} = (I_d + \delta_t \operatorname{div}(M(u^n)\nabla(\Delta + \alpha/\epsilon^2)))^{-1}$ , which cannot be made in Fourier space. Notice also that this approach has been recently proposed in [5, 40, 39] where the resolution of  $(u^{n+1}, \mu^{n+1})$  has been made using finite elements.

**Imex approach on the variational mobility term:** We then propose another approach in this paper keeping in mind the variational property of mobility:

$$\begin{cases} \partial_t u &= -\nabla_\mu J_u(\mu) \\ \mu &= \nabla_u \bar{E}_{u^n} \end{cases}$$

where

$$J_u(\mu) = \frac{1}{2} \int_Q M(u) |\nabla\mu|^2 dx.$$

As for the energy  $E$ , we then propose to split also  $J$  as the sum of a convex and a concave term  $J_u = J_{u,c} + J_{u,e}$  with respectively an implicit and explicit treatment of the convex and concave part:

$$\begin{cases} (u^{n+1} - u^n)/\delta_t &= -\nabla_\mu J_{u^n,c}(\mu^{n+1}) - \nabla_\mu J_{u^n,e}(\mu^n), \\ \mu^{n+1} &= \nabla_u E_c(u^{n+1}) + \nabla_u E_e(u^n). \end{cases}$$

As previously, this scheme can be interpreted as an Euler implicit discretization of

$$\begin{cases} \partial_t u &= -\nabla_\mu \bar{J}_{u^n,\mu^n}(\mu) \\ \mu &= \nabla_u \bar{E}_{u^n}, \end{cases}$$

where the new mobility energy  $\bar{J}_{u^n,\mu^n}$  is given by

$$\bar{J}_{u^n,\mu^n}(\mu) = J_{u^n,c}(\mu) + J_{u^n,e}(\mu^n) + \langle \nabla_\mu J_{u^n,e}(\mu^n), \mu - \mu^n \rangle.$$

Then, to ensure the decrease of  $t \mapsto \bar{E}_{u^n}(u(\cdot, t))$  along the flow, we require at least the semi-implicit metric  $\bar{J}_{u^n,\mu^n}$  to be non negative. This corresponds to the concavity condition on  $J_{u,e}$ , meaning that we have

$$0 \leq J_{u^n}(\mu) \leq \bar{J}_{u^n,\mu^n}(\mu).$$

Moreover, from the identity

$$\frac{d}{dt} \bar{E}_{u^n}(u) = \langle \nabla_u \bar{E}_{u^n}, u_t \rangle = -\langle \mu, \nabla_\mu \bar{J}_{u^n,\mu^n}(\mu) \rangle,$$

we conclude that it is sufficient to show that

$$\langle \mu, \nabla_\mu \bar{J}_{u^n,\mu^n}(\mu) \rangle \geq 0.$$

to ensure the decrease of the energy.

**Application to the M-CH model:** Motivated by the previous section, we propose the following splitting of  $J$ :

$$J_{u^n,c}(\mu) = \frac{1}{2} \int m |\nabla \mu|^2 dx \quad \text{and} \quad J_{u^n,e}(\mu) = \frac{1}{2} \int (M(u^n) - m) |\nabla \mu|^2 dx$$

with  $m > 0$ . We take  $m = \max_{s \in [0,1]} \{M(s)\}$  in order to obtain the concavity of  $J_{u^n,e}(\mu)$ , and the scheme reads

$$\begin{cases} (u^{n+1} - u^n)/\delta_t &= m \Delta \mu^{n+1} + \operatorname{div}((M(u^n) - m) \nabla \mu^n) \\ \mu^{n+1} &= \left(-\Delta u^{n+1} + \frac{\alpha}{\epsilon^2} u^{n+1}\right) + \left(\frac{1}{\epsilon^2} (W'(u^n) - \alpha u^n)\right), \end{cases}$$

or in a matrix form

$$\begin{pmatrix} I_d & -\delta_t m \Delta \\ \Delta - \alpha/\epsilon^2 & I_d \end{pmatrix} \begin{pmatrix} u^{n+1} \\ \mu^{n+1} \end{pmatrix} = \begin{pmatrix} u^n + \delta_t \operatorname{div}((M(u^n) - m) \nabla \mu^n) \\ \frac{1}{\epsilon^2} (W'(u^n) - \alpha u^n) \end{pmatrix} = \begin{pmatrix} B_{u^n, \mu^n}^1 \\ B_{u^n, \mu^n}^2 \end{pmatrix}$$

Finally, the couple  $(u^{n+1}, \mu^{n+1})$  can be expressed as

$$u^{n+1} = L_M \left[ B_{u^n, \mu^n}^1 + \delta_t m \Delta B_{u^n, \mu^n}^2 \right]$$

and

$$\mu^{n+1} = L_M \left[ (-\Delta B_{u^n, \mu^n}^1 + \alpha/\epsilon^2 B_{u^n, \mu^n}^1) + B_{u^n, \mu^n}^2 \right],$$

where the operator  $L_M$  is now given by  $L_M = (I_d + \delta_t m \Delta (\Delta - \alpha/\epsilon^2 I_d))^{-1}$ , which can be computed efficiently in Fourier space.

5.2.3. *Case of the NMN-CH model.* We now turn to the **NMN-CH** model:

$$\begin{cases} \partial_t u &= N(u) \operatorname{div}(M(u) \nabla(N(u) \mu)) \\ \mu &= \frac{1}{\epsilon^2} W'(u) - \Delta u, \end{cases}$$

where  $N(u) = \frac{1}{\sqrt{M(u)}}$  and  $M(u) = W(u) + \gamma \epsilon^2$ .

In a similar manner to the other models, we study the model rewritten in a variational form

$$\begin{cases} \partial_t u &= -\nabla_\mu J_u(\mu) \\ \mu &= \nabla_u \bar{E}_{u^n} \end{cases}$$

with

$$J_u(\mu) = \frac{1}{2} \int_Q M(u) |\nabla(N(u) \mu)|^2 dx.$$

$J_u$  can be split in three parts:

$$J_u(\mu) = \frac{1}{2} \int_Q |\nabla \mu|^2 dx + \int_Q G(u) \cdot \nabla \mu \mu dx + \frac{1}{2} \int_Q |G(u)|^2 \mu^2 dx,$$

with

$$G(u) = -\frac{1}{2} \nabla(\log(M(u)))$$

as  $N(u) = \frac{1}{\sqrt{M(u)}}$  and  $\sqrt{M(u)} \nabla(N(u)) = -\frac{1}{2} \frac{\nabla M(u)}{M(u)} = -\nabla(\log(M(u)))$ .

This suggests that we could use the following splitting of  $J_u(\mu) = J_{u,c}(\mu) + J_{u,e}(\mu)$  with

$$J_{u,c}(\mu) = \frac{1}{2} \int_Q m |\nabla \mu|^2 dx + \frac{1}{2} \int_Q \beta \mu^2 dx$$

and

$$J_{u,e}(\mu) = \int_Q G(u) \cdot \nabla \mu \mu dx + \frac{1}{2} \int_Q (|G(u)|^2 - \beta) \mu^2 dx + \frac{1}{2} \int_Q (1 - m) |\nabla \mu|^2 dx,$$

with  $\beta > 0$  and  $m > 0$ . Moreover, as soon as  $G(u)$  is bounded is  $H_1(Q)$ , a sufficiently large choice for  $m$  and  $\beta$  should ensure the concavity of  $J_{u,e}(\mu)$ . In practice, we take  $m = 1$  and

$\beta = 1/\epsilon^2$  for our numerical experiments and these values did not show any sign of instability regardless of the choice of the time step  $\delta_t$ . In particular, this leads to the following system

$$\begin{cases} (u^{n+1} - u^n)/\delta_t &= m\Delta\mu^{n+1} - \beta\mu^{n+1} + H(u^n, \mu^n) \\ \mu^{n+1} &= \left(-\Delta u^{n+1} + \frac{\alpha}{\epsilon^2}u^{n+1}\right) + \left(\frac{1}{\epsilon^2}(W'(u^n) - \alpha u^n)\right), \end{cases}$$

where

$$H(u^n, \mu^n) = N(u^n) \operatorname{div}((M(u^n)\nabla(N(u^n)\mu^n)) - m\Delta\mu^n + \beta\mu^n)$$

The couple  $(u^{n+1}, \mu^{n+1})$  is then solution of the system

$$\begin{pmatrix} I_d & -\delta_t(m\Delta - \beta I_d) \\ \Delta - \alpha/\epsilon^2 & I_d \end{pmatrix} \begin{pmatrix} u^{n+1} \\ \mu^{n+1} \end{pmatrix} = \begin{pmatrix} u^n + \delta_t H(u^n, \mu^n) \\ \frac{1}{\epsilon^2}(W'(u^n) - \alpha u^n) \end{pmatrix} = \begin{pmatrix} B_{u^n, \mu^n}^1 \\ B_{u^n, \mu^n}^2 \end{pmatrix}$$

satisfying

$$u^{n+1} = L_{NMN} \left[ B_{u^n, \mu^n}^1 + \delta_t(m\Delta B_{u^n, \mu^n}^2 - \beta B_{u^n, \mu^n}^2) \right]$$

and

$$\mu^{n+1} = L_{NMN} \left[ (-\Delta B_{u^n, \mu^n}^1 + \alpha/\epsilon^2 B_{u^n, \mu^n}^1) + B_{u^n, \mu^n}^2 \right].$$

Here the operator  $L_{NMN}$  is given by  $L_{NMN} = (I_d + \delta_t(m\Delta - \beta I_d)(\Delta - \alpha/\epsilon^2 I_d))^{-1}$ , which can be still computed efficiently in Fourier space.

**5.3. Matlab code.** We present in Figure (1) an example of **Matlab** script with less than 40 lines which implements the scheme approximating the solutions of the **NMN-CH** model. In particular :

- We consider here a computation box  $Q = [-1/2, 1/2]^2$  discretized with  $N = 2^9$  nodes in each direction. The initial condition of  $u$  is a uniform noise and the numerical parameters are given by  $\epsilon = 2/N$ ,  $\delta_t = 4\epsilon^2$ ,  $\alpha = 2$ ,  $\beta = 2/\epsilon^2$  and  $m = 1$ .
- Line 14 corresponds to the definition of the Fourier-symbol associated with operator  $L_{NMN}$ . The application of  $L_{NMN}$  can then be performed using a simple multiplication in Fourier space with the array  $M_{LNMN}$ .
- The computation of  $N(u) \operatorname{div}(M(u)\nabla(N(u)\mu))$  is made on line 28 and is based on the following equality

$$\begin{aligned} N(u) \operatorname{div}(M(u)\nabla(N(u)\mu)) &= \sqrt{M(u)}\Delta N(u)\mu + N(u)\nabla(M(u)) \cdot \nabla(N(u)\mu) \\ &= \sqrt{M(u)}\Delta N(u)\mu + 2\nabla \left[ \sqrt{M(u)} \right] \cdot \nabla(N(u)\mu), \end{aligned}$$

as  $N = 1/\sqrt{M(u)}$ .

- Each computation of gradient and divergence operator are made in Fourier space. For instance the gradient of  $\sqrt{M(u)}$  is computed on line 23.
- Figure (2) shows the phase field function  $u^n$  computed at different times  $t^n$  by using this script.

We believe that this implementation shows the simplicity, efficiency and stability of our numerical scheme.

**5.3.1. Asymptotic expansion and flow: numerical comparison of the different models.** The first numerical example concerns the evolution of an initial connected set. For each Cahn–Hilliard model, we plot on figure (3) the phase field function  $u^n$  computed at different times  $t$ . Each experiment is performed using the same numerical parameters:  $\delta_x = \frac{1}{2^8}$ ,  $\epsilon = 2\delta_x$ ,  $\delta_t = \epsilon^4$ ,  $\alpha = 2/\epsilon^2$ ,  $m = 1$ , and  $\beta = 2/\epsilon^2$ . The first, second and third lines on (3) correspond respectively to the solution  $u$  given by the **C-CH** model, the **M-CH** model and the **NMN-CH** model. The first remark is that, as expected, the **C-CH** model, whose limit flow is the Hele-Shaw model [35, 3]) gives a slightly different flow compared to the other two models. On the other hand, the numerical experiments obtained using the **M-CH** model and the **NMN-CH** model are very similar and should give a good approximation of the surface diffusion flow. In addition, for each

```

1 clear all;
2 %%%%%%%%% Numerical parameters %%%%%%%%%
3 N = 2^9; epsilon =1/N; dt =epsilon^4; T =1;
4 %%%%%%%%% Double well potential, mobilities %%%%%%%%%
5 W = @(U) 1/2*(U.*(U-1)).^2;
6 W_prim = @(U) (U.*(U-1).*(2*U-1));
7 MobM = @(U) 1/2*(((U).*(1-U)).^2+epsilon^2) );
8 MobN = @(U) 1./sqrt(MobM(U) );
9
10 %%%%%%%%% Fourier operators %%%%%%%%%
11 k = [0:N/2,-N/2+1:-1]; [K1,K2] = meshgrid(k,k);
12 Delta = -4*pi^2*((K1.^2 + (K2).^2));
13 alpha = 2; beta = 1/epsilon^2; m = 1;
14 M_LNMN = 1./(1 + dt*(m*Delta - beta) .*(Delta - alpha/epsilon^2));
15
16 %%%%%%%%% Initial condition %%%%%%%%%
17 U = rand(N,N); U_fourier = fft2(U);
18 Mu = zeros(N,N); Mu_fourier = zeros(N,N);
19 %%%%%%%%% Scheme loop %%%%%%%%%
20 for i=1:T/dt,
21 mobMU = MobM(U); mobNU = MobN(U);
22 sqrtM = sqrt(mobMU); sqrtM_fourier = fft2(sqrtM);
23 nabla1_sqrtM= real(ifft2(2*pi*i*K1.*sqrtM_fourier )); nabla2_sqrtM= real(ifft2(2*pi*i
    i*K2.*sqrtM_fourier ));
24
25 muN_fourier = fft2(Mu.*mobNU); muN = real(ifft2(muN_fourier));
26 nabla1_muN = real(ifft2(2*pi*i*K1.*muN_fourier )); nabla2_muN = real(ifft2(2*pi*i*K2
    .*muN_fourier ));
27 laplacien_muN = real(ifft2(Delta.*muN_fourier ));
28 NdivMgradNMu = sqrtM.*laplacien_muN + 2*(nabla1_sqrtM.*nabla1_muN +nabla2_sqrtM.*
    nabla2_muN);
29
30 B1 = U_fourier + dt*(fft2(NdivMgradNMu) - (m*Delta-beta).*Mu_fourier);
31 B2 = fft2(W_prim(U)/epsilon^2 - alpha/epsilon^2*U);
32
33 U_fourier = M_LNMN.*(B1 + dt*(m*Delta-beta).*B2);
34 U = real(ifft2(U_fourier));
35 Mu_fourier = M_LNMN.*(alpha/epsilon^2 - Delta).*B1 + B2);
36 Mu = real(ifft2(Mu_fourier));
37
38 end

```

FIGURE 1. Example of **Matlab** implementation of the previous scheme in dimension 2 to approximate the solutions to the **NMN-CH** model.

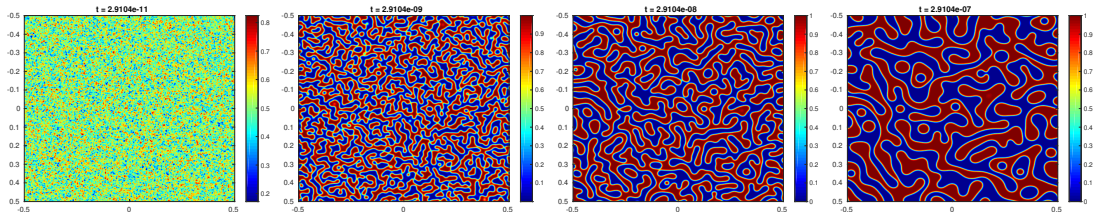


FIGURE 2. First numerical experiment using the **NMN-CH** model; the solutions  $u$  are computed with the **Matlab** script of Figure 1.

model, the stationary flow limit appears to correspond to a ball of the same mass as that of the initial set.

To illustrate the asymptotic expansion performed in Section 4, we plot on (4) (first two pictures) the slice  $x_1 \mapsto u(x_1, 0)$  at the final time  $T = 10^{-4}$ . The profil associated to the **C-CH** model is plotted in red and clearly indicates that the solution  $u$  does not remain in the interval  $[0, 1]$  with an overshoot of order  $O(\varepsilon)$ . As for the **M-CH** model (in blue), we can also observe a perturbation of order  $O(\varepsilon)$  of the best profile  $q(z)$  and  $u$  does not remain in  $[0, 1]$ . In contrast, the profile obtained using the **NMN** model (in green) seems to be very close to  $q$  and remains in  $[0, 1]$  up to an error of order  $O(\varepsilon^2)$ . Finally, we plot the evolution of the Cahn–Hilliard energy along the flow for each model on the last picture of (4). We can clearly observe a decrease of the energy in each case.

In conclusion, this first numerical experiment confirms the asymptotic expansion obtained in the previous section, and highlights the interest of our **NMN** model to approximate surface diffusion flows.

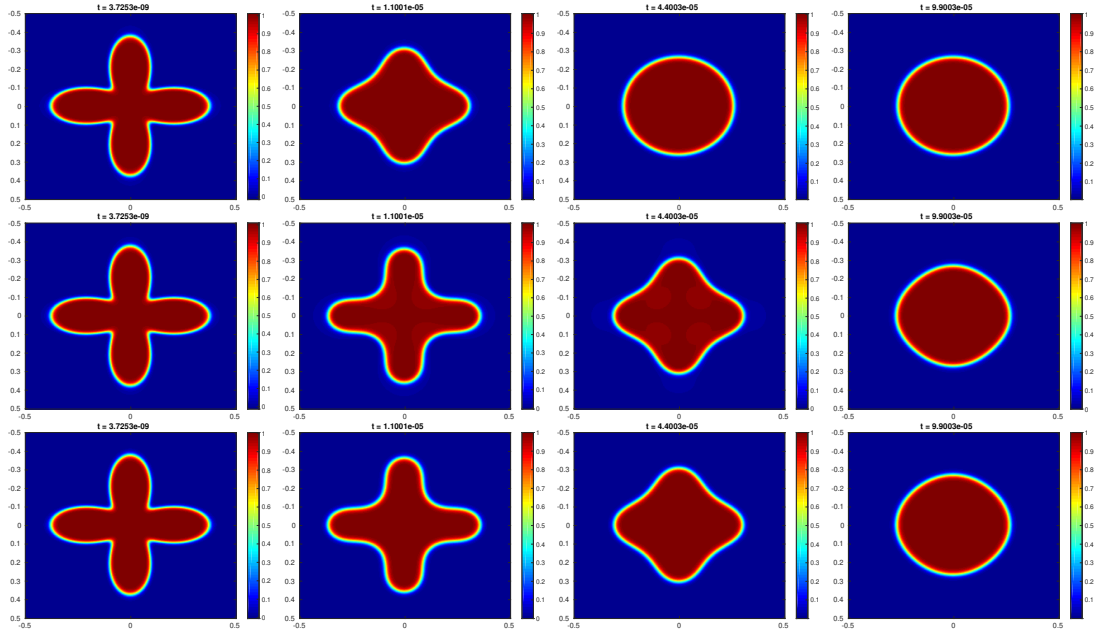


FIGURE 3. First numerical comparison of the three different **CH** models: Evolution of  $u$  along the iterations; First line using the **C-CH** model, Second line, using the **M-CH** model; last line using the **NMN-CH** model.

5.3.2. *Influence of the mobility: a local conservation of mass.* The second numerical experiment is intended to show the advantage of adding mobility to the classical Cahn–Hilliard model to preserve a local conservation of the mass. As previously, we use the same numerical parameter in each case:  $\delta_x = \frac{1}{2^8}$ ,  $\epsilon = 2/N$ ,  $\delta_t = \epsilon^4$ ,  $\alpha = 2/\epsilon^2$ ,  $m = 1$ , and  $\beta = 2/\epsilon^2$ . Then we plot on figure (5) the phase field function  $u$  obtained at different times  $t$  using the different phase field models (first line: **C-CH** model, second line: **M-CH** model, third line **NMN-CH** model). Here, the initial set is a disjoint union of five small sets. As expected, the evolutions obtained using the **M-CH** and the **NMN-CH** models show an independent evolution of each small disjoint set that converges to a ball of equivalent volume. This last point is clearly not the case using the **C-CH** model where the limit appears to be the union of three balls only. It suggests that the mass of the smaller set moves towards the larger set. This emphasizes the interest of adding mobility in the Cahn–Hilliard model to get a local conservation of mass, which is particularly relevant for various physical applications, for example the simulation of dewetting phenomena.

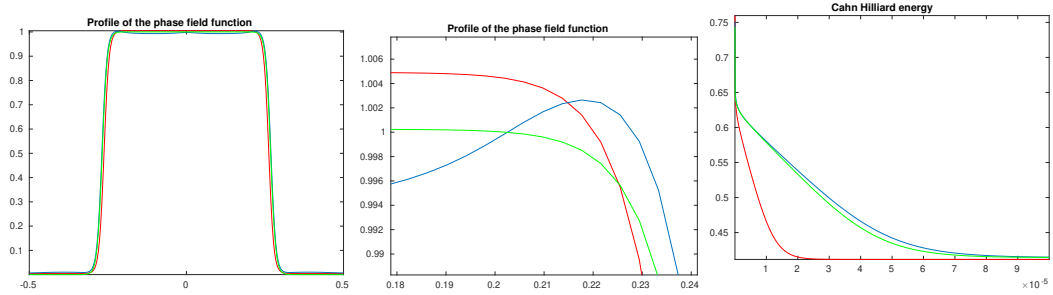


FIGURE 4. Comparison of the three different models: profil and energy; C-CH model in red, M-CH model in blue, NMN-CH model in green; First figure: slice of  $u$ :  $x_1 \mapsto u(x_1, 0)$ ; Second figure: zoom on the slice of  $u$ ; last figure: evolution of the Cahn–Hilliard energy along the flow.

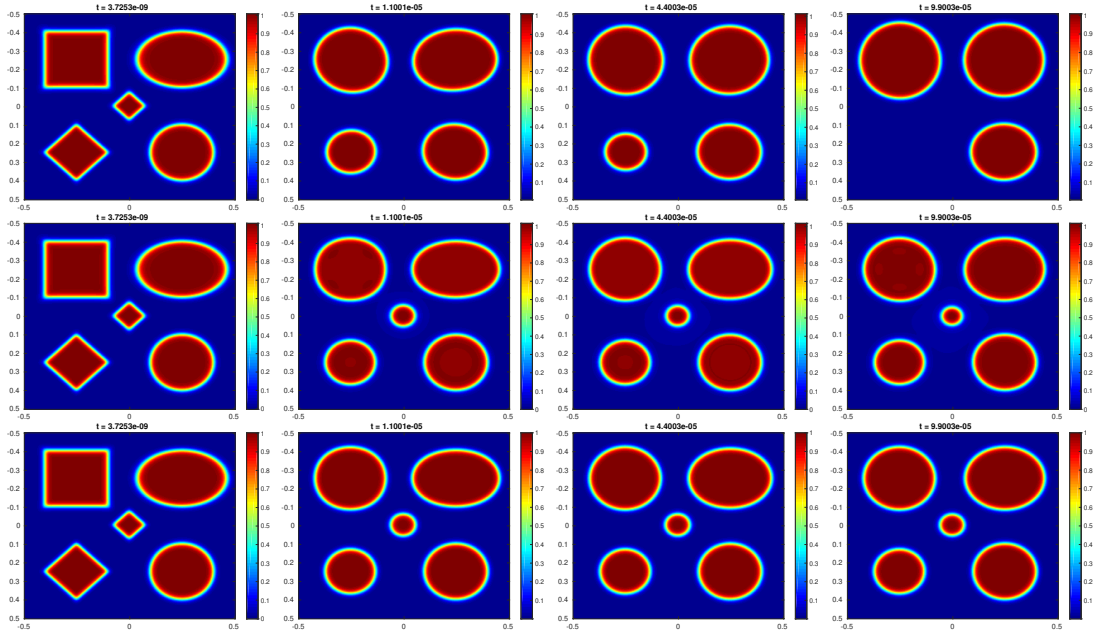


FIGURE 5. Numerical comparison of the three different phase field models: Local conservation of the mass; Evolution of  $u$  along the iterations; First line with the **C-CH** model. Second line with the **M-CH** model; Last line with the **NMN-CH** model.

5.3.3. *Numerical experiments with thin structures in dimension 3.* We propose now a numerical experiment in dimension 3 where the initial set is a thin tube. Our motivation here is to show the importance of having a model of order 2 in the phase field function  $u$  in the complicated case of a thin structure evolution. Similarly to the previous computations, the numerical parameters are given by  $\delta_x = \frac{1}{28}$ ,  $\epsilon = 2/N$ ,  $\delta_t = \epsilon^4$ ,  $\alpha = 2/\epsilon^2$ ,  $m = 1$ , and  $\beta = 2/\epsilon^2$ . We plot on each picture of (6) the  $1/2$ -level set of  $u$  for different times  $t$ . The first, second and third line correspond, respectively, to the **C-CH**, **M-CH** and **NMN-CH** models. We observe that the evolutionary set disappears using the **C-CH** and **M-CH** models whereas the **NMN-CH** model seems to have better volume conservation properties and the stationary set is given as the sum of five small spheres.

The results are surprising at first glance as the mass of  $u$  ( $\int_Q u dx$ ) is well preserved using the **C-CH** and **M-CH** models. So, to convince oneself that the problem arises from the phase field model order and not the numerical discretization, we plot on figure (7) the numerical evolution of the mass  $t \mapsto \int_Q u dx$  along the flow for each model. We observe a very good conservation in the case of **C-CH** and **M-CH** models despite the disappearance of the structure.

Moreover, recall that we plot on figure (6) the 1/2-level set of  $u$ :

$$\Omega_\epsilon(t) = \{x \in Q; u(x, t) \leq 1/2\},$$

and that for a phase field model of order 1 only, we have

$$Vol(\Omega_\epsilon(t)) = \int_Q u(x, t) dx + O(\epsilon).$$

This means that even if the mass of  $u$  is conserved, we observe an error of order  $O(\epsilon)$  on the volume of  $\Omega_\epsilon$ . The consequence is all the more dramatic in our example as the volume of the thin structure is of order  $\epsilon^2$ . In the end, the whole volume is lost because of this approximation error. Concerning the **NMN-CH** model, we proved a volume approximation of order 2,

$$Vol(\Omega_\epsilon(t)) = \int_Q u(x, t) dx + O(\epsilon^2),$$

This explains the good numerical behavior of the **NMN-CH** model in comparison with the other models.

In conclusion, this 3D numerical experiment showcases the inefficiency of models **C-CH** and **M-CH** to approximate the evolution of a thin structure, where a much smaller  $\epsilon$  is required. On the other hand, the second order **NMN-CH** phase field model seems to give a good approximation of surface diffusion even if the mass of  $u$  is not perfectly conserved (Green plot on Figure (7)).

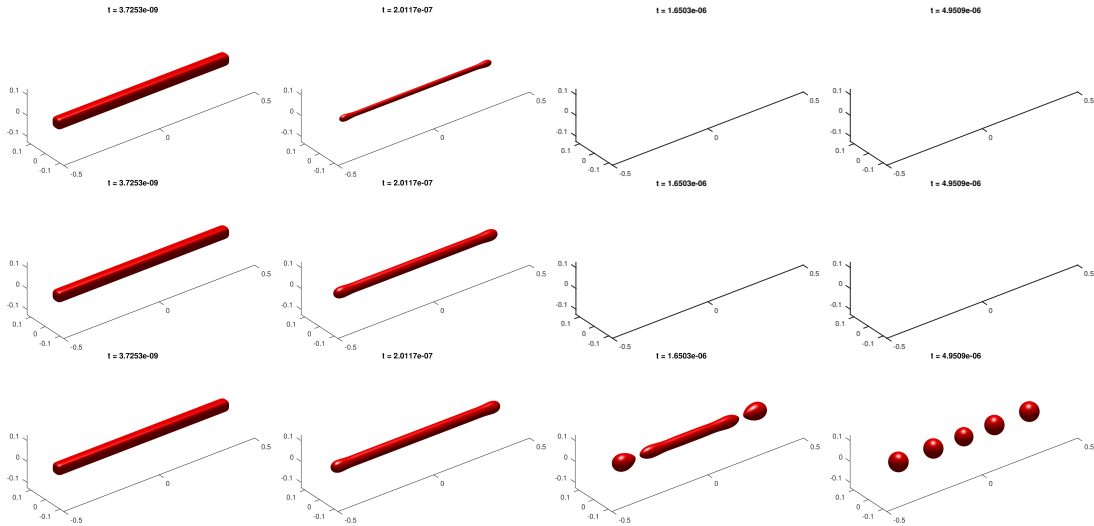


FIGURE 6. Comparison of the different models in the case of a thin structure in dimension 3. First line corresponds to the **C-CH** model, second line to the **M-CH** model, and third line to the **NMN-CH** model.

5.3.4. *Dewetting and surface diffusion of a thin plate.* The last numerical example is the evolution of a thin plate using the **NMN-CH** model. As previously, the parameters are chosen as  $\delta_x = \frac{1}{28}$ ,  $\epsilon = 2/N$ ,  $\delta_t = \epsilon^4$ ,  $\alpha = 2/\epsilon^2$ ,  $m = 1$ , and  $\beta = 2/\epsilon^2$ . We can observe on figure (8) an evolution similar to the one observed in real dewetting experiments[5].

#### ACKNOWLEDGMENT

The authors thank Roland Denis for fruitful discussions. They acknowledge support from the French National Research Agency (ANR) under grants ANR-18-CE05-0017 (project BEEP) and ANR-19-CE01-0009-01 (project MIMESIS-3D). Part of this work was also supported by the LABEX MILYON (ANR-10-LABX-0070) of Université de Lyon, within the program "Investissements d'Avenir" (ANR-11-IDEX- 0007) operated by the French National Research Agency (ANR).

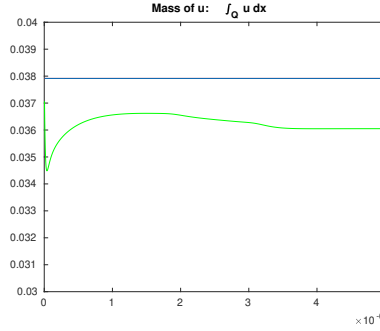


FIGURE 7. Comparison of the different models in the case of a thin structure in dimension 3. Evolution of the mass of  $u$  given by  $\int u dx$  along the iterations; Using the **C-CH** model in red, the **M-CH** model in blue, and the **NMN-CH** model in green.

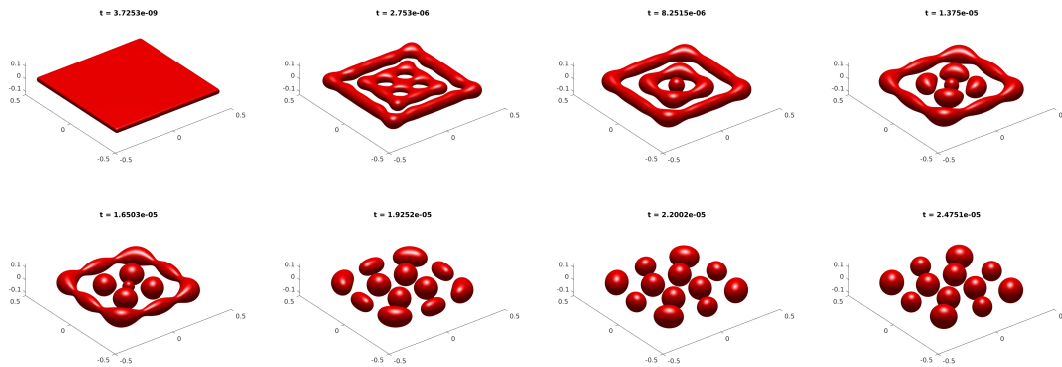


FIGURE 8. Example of dewetting in dimension 3 using the **NMN-CH** model. Evolution of  $u$  along the iterations.

## REFERENCES

- [1] Marco Albani, Roberto Bergamaschini, and Francesco Montalenti. Dynamics of pit filling in heteroepitaxy via phase-field simulations. *Physical Review B*, 94(7):075303, 2016. [2](#)
- [2] Matthieu Alfaro and Pierre Alifrangis. Convergence of a mass conserving Allen-Cahn equation whose Lagrange multiplier is nonlocal and local. *arXiv preprint arXiv:1303.3553*, 2013. [8](#), [13](#)
- [3] Nicholas D Alikakos, Peter W Bates, and Xinfu Chen. Convergence of the Cahn-Hilliard equation to the Hele-Shaw model. *Archive for Rational Mechanics and Analysis*, 128(2):165–205, 1994. [1](#), [13](#), [19](#)
- [4] L. Ambrosio. Geometric evolution problems, distance function and viscosity solutions. *Calculus of variations and partial differential equations* (Pisa, 1996), 5–93, 2000. [8](#), [9](#)
- [5] Rainer Backofen, Steven M. Wise, Marco Salvalaglio, and Axel Voigt. Convexity splitting in a phase field model for surface diffusion. *Int. J. Numer. Anal. Model.*, 16(2):192–209, 2019. [15](#), [17](#), [23](#)
- [6] Andrea Bertozzi, Selim Esedoglu, and Alan Gillette. inpainting of binary images using the Cahn-Hilliard equation. *Image Processing, IEEE Transactions on*, 16:285 – 291, 02 2007. [1](#)
- [7] Franck Boyer, Celine Lapuerta, Sebastian Minjeaud, Bruno Piar, and Michel Quintard. Cahn-Hilliard Navier-Stokes model for the simulation of three-phase flows. 04 2010. [1](#)
- [8] Franck Boyer and Flore Nabet. A DDFV method for a Cahn-Hilliard/Stokes phase field model with dynamic boundary conditions. *ESAIM: Mathematical Modelling and Numerical Analysis*, 51, 11 2016. [1](#)
- [9] M. Brassel and E. Bretin. A modified phase field approximation for mean curvature flow with conservation of the volume. *Mathematical Methods in the Applied Sciences*, 34(10):1157–1180, 2011. [3](#), [7](#), [15](#)
- [10] Elie Bretin, Alexandre Danescu, José Penuelas, and Simon Masnou. Multiphase mean curvature flows with high mobility contrasts: A phase-field approach, with applications to nanowires. *Journal of Computational Physics*, 365:324–349, 2018. [15](#)
- [11] Elie Bretin and Simon Masnou. A new phase field model for inhomogeneous minimal partitions, and applications to droplets dynamics. *Interfaces and Free Boundaries*, 19:141–182, 01 2017. [15](#)
- [12] Elie Bretin, Simon Masnou, and Édouard Oudet. Phase-field approximations of the Willmore functional and flow. *Numer. Math.*, 131(1):115–171, 2015. [8](#)



- [13] E. Bretin, R. Denis, J.-O. Lachaud, and E. Oudet. Phase-field modelling and computing for a large number of phases. *ESAIM: M2AN*, 53(3):805–832, 2019. [3](#), [15](#)
- [14] Martin Burger, Lin He, and Carola-Bibiane Schönlieb. Cahn-Hilliard inpainting and a generalization for grayvalue images. *SIAM J. Imaging Sciences*, 2:1129–1167, 01 2009. [1](#)
- [15] John W. Cahn. On spinodal decomposition. *Acta Metallurgica*, 9(9):795–801, 1961. [1](#)
- [16] John W Cahn, Charles M Elliott, and Amy Novick-Cohen. The Cahn-Hilliard equation with a concentration dependent mobility: motion by minus the Laplacian of the mean curvature. *European journal of applied mathematics*, 7(3):287–301, 1996. [1](#)
- [17] John W. Cahn and John E. Hilliard. Free energy of a nonuniform system. I. Interfacial free energy. *The Journal of Chemical Physics*, 28(2):258–267, 1958. [1](#)
- [18] L.Q. Chen and Jie Shen. Applications of semi-implicit Fourier-spectral method to phase field equations. *Computer Physics Communications*, 108:147–158, 1998. [15](#)
- [19] Xinfu Chen, Danielle Hilhorst, and Elisabeth Logak. Mass conserving Allen-Cahn equation and volume preserving mean curvature flow. *Interfaces and Free Boundaries*, 12(4):527–549, 2011. [8](#)
- [20] Mowei Cheng and James A. Warren. An efficient algorithm for solving the phase field crystal model. *J. Comput. Phys.*, 227(12):6241–6248, 2008. [15](#)
- [21] Laurence Cherfils, Hussein Fakhri, and Alain Miranville. A complex version of the Cahn-Hilliard equation for grayscale image inpainting. *Multiscale Modeling and Simulation*, 15:575–605, 03 2017. [1](#)
- [22] Shibin Dai and Qiang Du. Motion of interfaces governed by the Cahn-Hilliard equation with highly disparate diffusion mobility. *SIAM Journal on Applied Mathematics*, 72(6):1818–1841, 2012. [2](#)
- [23] Shibin Dai and Qiang Du. Coarsening mechanism for systems governed by the Cahn-Hilliard equation with degenerate diffusion mobility. *Multiscale Modeling & Simulation*, 12(4):1870–1889, 2014. [2](#)
- [24] Qiang Du and Xiaobing Feng. Chapter 5 - the phase field method for geometric moving interfaces and their numerical approximations. In Andrea Bonito and Ricardo H. Nochetto, editors, *Geometric Partial Differential Equations - Part I*, volume 21 of *Handbook of Numerical Analysis*, page 425–508. Elsevier, 2020. [15](#)
- [25] Marion Dziwnik, Andreas Münch, and Barbara Wagner. An anisotropic phase-field model for solid-state dewetting and its sharp-interface limit. *Nonlinearity*, 30(4):1465, 2017. [2](#)
- [26] Matt Elsey and Benedikt Wirth. A simple and efficient scheme for phase field crystal simulation. *ESAIM Math. Model. Numer. Anal.*, 47(5):1413–1432, 2013. [15](#)
- [27] David J. Eyre. Unconditionally gradient stable time marching the Cahn-Hilliard equation. In *Computational and mathematical models of microstructural evolution (San Francisco, CA, 1998)*, volume 529 of *Mater. Res. Soc. Sympos. Proc.*, pages 39–46. MRS, Warrendale, PA, 1998. [15](#), [16](#)
- [28] Hector Gomez and Thomas J. R. Hughes. Provably unconditionally stable, second-order time-accurate, mixed variational methods for phase-field models. *J. Comput. Phys.*, 230(13):5310–5327, 2011. [15](#)
- [29] Clemens Gugenberger, Robert Spatschek, and Klaus Kassner. Comparison of phase-field models for surface diffusion. *Physical Review E*, 78(1):016703, 2008. [2](#)
- [30] Alpha A Lee, Andreas Münch, and Endre Süli. Degenerate mobilities in phase field models are insufficient to capture surface diffusion. *Applied Physics Letters*, 107(8):081603, 2015. [2](#)
- [31] Alpha Albert Lee, Andreas Munch, and Endre Suli. Sharp-interface limits of the Cahn-Hilliard equation with degenerate mobility. *SIAM Journal on Applied Mathematics*, 76(2):433–456, 2016. [2](#), [4](#)
- [32] Alain Miranville. *The Cahn-Hilliard Equation: Recent Advances and Applications*. 08 2019. [1](#)
- [33] Meher Naffouti, Rainer Backofen, Marco Salvalaglio, Thomas Bottein, Mario Lodari, Axel Voigt, Thomas David, Abdelmalek Benkouider, Ibtissem Fraj, Luc Favre, et al. Complex dewetting scenarios of ultrathin silicon films for large-scale nanoarchitectures. *Science advances*, 3(11):eaao1472, 2017. [2](#)
- [34] Amy Novick-Cohen. The Cahn-Hilliard equation. *Handbook of differential equations: evolutionary equations*, 4:201–228, 2008. [1](#)
- [35] Robert L Pego. Front migration in the nonlinear Cahn-Hilliard equation. *Proceedings of the Royal Society of London. A. Mathematical and Physical Sciences*, 422(1863):261–278, 1989. [1](#), [19](#)
- [36] Andreas Rätz, Angel Ribalta, and Axel Voigt. Surface evolution of elastically stressed films under deposition by a diffuse interface model. *Journal of Computational Physics*, 214(1):187–208, 2006. [2](#)
- [37] Marco Salvalaglio, Rainer Backofen, Roberto Bergamaschini, Francesco Montalenti, and Axel Voigt. Faceting of equilibrium and metastable nanostructures: a phase-field model of surface diffusion tackling realistic shapes. *Crystal Growth & Design*, 15(6):2787–2794, 2015. [2](#)
- [38] Marco Salvalaglio, Rainer Backofen, Axel Voigt, and Francesco Montalenti. Morphological evolution of pit-patterned Si (001) substrates driven by surface-energy reduction. *Nanoscale research letters*, 12(1):554, 2017. [2](#)
- [39] Marco Salvalaglio, Maximilian Selch, Axel Voigt, and Steven Wise. Doubly degenerate diffuse interface models of anisotropic surface diffusion. 04 2020. [15](#), [17](#)
- [40] Marco Salvalaglio, Axel Voigt, and Steven M Wise. Doubly degenerate diffuse interface models of surface diffusion. *arXiv preprint arXiv:1909.04458*, 2019. [2](#), [3](#), [5](#), [15](#), [17](#)

- [41] Jaemin Shin, Hyun Geun Lee, and June-Yub Lee. First and second order numerical methods based on a new convex splitting for phase-field crystal equation. *J. Comput. Phys.*, 327:519–542, 2016. [15](#)
- [42] Jaemin Shin, Hyun Geun Lee, and June-Yub Lee. Unconditionally stable methods for gradient flow using convex splitting Runge-Kutta scheme. *J. Comput. Phys.*, 347:367–381, 2017. [15](#)
- [43] S. M. Wise, C. Wang, and J. S. Lowengrub. An energy-stable and convergent finite-difference scheme for the phase field crystal equation. *SIAM J. Numer. Anal.*, 47(3):2269–2288, 2009. [15](#)

UNIV LYON, INSA DE LYON, CNRS UMR 5208, INSTITUT CAMILLE JORDAN, 20 AVENUE ALBERT EINSTEIN, F-69621 VILLEURBANNE, FRANCE, ELIE.BRETIN@INSA-LYON.FR

UNIV LYON, UNIVERSITÉ CLAUDE BERNARD LYON 1, CNRS UMR 5208, INSTITUT CAMILLE JORDAN, 43 BOULEVARD DU 11 NOVEMBRE 1918, F-69622 VILLEURBANNE, FRANCE, MASNOU@MATH.UNIV-LYON1.FR

UNIV LYON, UNIVERSITÉ CLAUDE BERNARD LYON 1, CNRS UMR 5208, INSTITUT CAMILLE JORDAN, 43 BOULEVARD DU 11 NOVEMBRE 1918, F-69622 VILLEURBANNE, FRANCE, SENGER@MATH.UNIV-LYON1.FR

UNIV LYON, UNIVERSITÉ CLAUDE BERNARD LYON 1, CNRS UMR 5208, INSTITUT CAMILLE JORDAN, 43 BOULEVARD DU 11 NOVEMBRE 1918, F-69622 VILLEURBANNE, FRANCE, TERII@MATH.UNIV-LYON1.FR